

INSTITUTE FOR DIRECT ENERGY CONVERSION

TOWNE SCHOOL

UNIVERSITY OF PENNSYLVANIA

PHILADELPHIA, PENNSYLVANIA

MANFRED ALTMAN, DIRECTOR

STATUS REPORT

INDEC-SR-13

NATIONAL AERONAUTICS AND SPACE ADMINISTRATION

GRANT NSG - 316

December 1967

INTRODUCTION

At the present time, the Institute has twenty-seven participants. Of these, nine are of professional rank, three are post-doctoral researchers, thirteen are Ph.D. candidates, and two are M.S. candidates.

During Calendar 1967-1968, five Ph.D.'s have been granted to Institute participants.

The technical work of the Institute has resulted in thirty papers in archive journals, twenty papers in major Conference Proceedings, and six invited addresses since its inception in 1962.

The first part of this report contains a summary of projects and details are included in the Appendix.

TABLE OF CONTENTS

✓ 1. MATERIALS ENGINEERING

- 1.1 High Temperature Thermal Diffusivity Measurement
 - Objectives, progress, and accomplishments to date 1-2
 - Details of progress for period 1 July to 31 December 1967 A1-1
- 1.2 Thermoelectric Properties of Graphite Alloys
 - Objectives, progress, and accomplishments to date 1-4
- 1.3 Superconductivity in Evaporated Tungsten Films
 - Objectives, progress, and accomplishments to date 1-7
 - Details of progress for period 1 July to 31 December 1967 A1-15
- 1.4 Studies of Thermal Transpiration for the Development of a "Thermal Pump"
 - Objectives, progress, and accomplishments to date 1-8
 - Details of progress for period 1 July to 31 December 1967 A1-23
- 1.5 Thermoelectric Properties of Graphite Compounds
 - Objectives, progress, and accomplishments to date 1-9
 - Details of progress for period 1 July to 31 December 1967 A1-31

✓ 2. PLASMA ENGINEERING

- 2.1 Flow of a Conducting Liquid in an Annular Gap: Experimental and Theoretical Study
 - Objectives, progress, and accomplishments to date 1-10
- 2.2 Basic Surface Investigations
 - Objectives, progress, and accomplishments to date 1-11
- 2.3 A Materials Study of Silicon Solar Cells
 - Objectives, progress, and accomplishments to date 1-13

3. ELECTROCHEMICAL ENGINEERING

3.1 Overpotential Transients on the Rotating Disk

Objectives, progress, and accomplishments to date 1-14

Details of progress for period 1 July to 31 December 1967 A3-1

3.2 Current and Potential Distribution in Cylindrical Geometries: Engineering Application to Fuel Cell Design

Objectives, progress, and accomplishments to date 1-16

Details of progress for period 1 July to 31 December 1967 A3-4

3.3 Foaming Electrolyte Fuel Cell

Objectives, progress, and accomplishments to date 1-18

Details of progress for period 1 July to 31 December 1967 A3-9

3.4 Atomic Scale Electrode Processes

Objectives, progress, and accomplishments to date 1-19

Details of progress for period 1 July to 31 December 1967 A3-13

3.5 Primary and Secondary Cells using Charge Transfer Complexes

Objectives, progress, and accomplishments to date 1-20

Details of progress for period 1 July to 31 December 1967 A3-20

3.6 Boiling Fuel Cell

Objectives, progress, and accomplishments to date 1-21

4. PUBLICATIONS

N 68 - 21036

1. MATERIALS ENGINEERING

Branch Chief: Dr. Manfred Altman

Senior Members: Dr. Solomon Pollack, Dr. Louis Girifalco

1.1 High Temperature Thermal Diffusivity Measurement

Senior Investigator: Dr. Manfred Altman

Post-doctoral Fellow: Dr. K. Sreenivasan

OBJECTIVES

To develop an experimental technique for the determination of thermal diffusivity of thermal energy storage materials in the liquid state.

PREVIOUS ACCOMPLISHMENTS

Phase 1: The theory of transient technique was studied and a new technique applicable to liquids was developed.

Phase 2: The furnace and the measuring equipment were designed and built.

Phase 3: The thermal diffusivity of the container material, boron nitride, was measured.

Phase 4: The thermal diffusivity of liquid lithium fluoride was measured.

Phase 5: The method and the cell were calibrated by measuring the thermal diffusivity of liquid sodium nitrate.

Phase 6: The thermal diffusivity of lithium fluoride in the solid and the liquid state were compared and an empirical correlation for the thermal conductivity at the melting point was developed. A doctoral dissertation based on this work was completed. This dissertation (Ref. 5) constitutes a final report on the project. Details are presented on page A1-1 through A1-9.

1.1 High Temperature Thermal Diffusivity Measurement

Senior Investigator: Dr. Manfred Altman

Graduate Student: H. Keramaty

OBJECTIVES

To develop experimental techniques suitable for the measurement of thermal diffusivity of solid mixtures. Primarily for the determination of the diffusivity of materials which do not lend themselves to large physical samples to be measured directly.

PREVIOUS ACCOMPLISHMENTS

A vacuum furnace which was designed, built and checked, was utilized to measure the thermal diffusivities of CaF_2 , BaF_2 and two of their mixtures. The thermal diffusivities of MgF_2 and a mixture of it with CaF_2 was also measured and reported in INDEC-SR-12.

PROGRESS IN PAST PERIOD

More samples of MgF_2 , CaF_2 and their mixtures (1 to 1 weight) and also 2 MgF_2 + 1 CaF_2 by weight were tested and except for the last mixture which is a new addition to the list, the results agreed well with the ones reported in INDEC-SR - 11 and 12. (Details appear on Fig. 1 and Table 1, pgs. A1-10 and A1-11).

1.2 Experimental Determination of the Thermoelectric Properties of Graphite Alloys

Senior Investigator: Dr. S. R. Pollack

Graduate Student: J. J. Curry

Objectives

The aim of this project is to study several compounds belonging to the class $I - II_2 - III - VI_4$. The four compounds chosen for study as potential thermoelectric materials are:

1. $Cu Cd_2 In Te_4$
2. $Cu Zn_2 In Te_4$
3. $Cu Cd_2 In Se_4$
4. $Cu Zn_2 In Se_4$

Experiments are to be performed on the above mentioned compounds to try and characterize their thermoelectric properties as completely as possible.

Previous Accomplishments

As reported in INDEC-SR-12, equipment has been constructed to measure the thermoelectric power, electrical conductivity and Hall coefficient. Techniques have been developed for the reproducible production of the compounds. Conductivity and thermoelectric power data for $Cu Cd_2 In Te_4$ were presented.

Progress in Past Period

Hall coefficient studies along with electrical conductivity measurements have been completed for both $\text{Cu Cd}_2 \text{ In Te}_4$ and $\text{Cu Zn}_2 \text{ In Te}_4$. A comparison of their properties at 300°K is shown in Table I. Figures I and II show plots of the resistivity and thermoelectric power as a function of temperature for each of the compounds. Both compounds show high thermoelectric powers, high resistivities and very low carrier mobilities. The temperature dependence of the mobility is not characteristic of a single scattering mechanism. The low mobility may be due to a complex valence band structure, and this possibility is currently being investigated theoretically. Optical reflection measurements were made over the range 6000Å--25000Å on both compounds and no characteristic absorptions were noted. Knoop microhardness measurements were made to see the effects of the variation in lattice parameter on hardness, and these results are shown in Table I. Z-meter measurements could not be made with sufficient accuracy or reproducibility to be meaningful due to the high vapor pressures of Cd, Zn and Te. In addition the values of the resistivity in the range 1.1°K -- 4.2°K have been measured for both compounds.

Future Work

Identical measurements will be carried out on $\text{Cu Cd}_2 \text{ In Se}_4$ and $\text{Cu Zn}_2 \text{ In Se}_4$. As mentioned earlier, the values of the TEP and resistivity may be able to be explained by a complex valence band structure and the details of this structure are currently under scrutiny.

General Considerations

Even though the thermoelectric power of these compounds is high, their low carrier mobility precludes their possible use as thermoelectric materials, provided that the mobility could not be improved by suitable doping techniques.

1.3 SUPERCONDUCTIVITY IN EVAPORATED TUNGSTEN FILMS

Senior Investigator: Dr. S. R. Pollack

Graduate Student: S. Basavaiah

Objectives

The primary objective is to study the superconducting properties of tungsten thin films by structural analysis and by electron tunneling in superconducting junctions.

Previous Accomplishments

Electron transfer in tungsten-tungsten oxide-gold thin film junctions was studied with the aim of developing a suitable tunnel emission cold cathode structure. From the study of a number of such junctions, the following conclusions were reached. (a) Current flow in these junctions is not by tunneling alone. (b) Large temperature dependence of current indicates processes other than tunneling, such as Schottky emission. (c) Barrier heights are much less than 1 eV which makes the tungsten system unsuitable for tunnel emission cathode. (d) Tungsten films superconduct at 3.2°K as compared to the bulk value of $.01^{\circ}\text{K}$.

Progress in Past Period

The structure of tungsten films was studied by x-ray and electron diffraction techniques. β -W (A15) phase was observed for films prepared at 10^{-6} torr, whereas for films prepared at 10^{-9} torr only the α -W (B.C.C.) structure was found. Transition temperature T_c for films prepared at 10^{-6} torr is 3.2°K , whereas films prepared at 10^{-9} torr did not superconduct down to 1.1°K . Superconducting tunneling data was obtained for $\text{W-W}_{x-y}\text{O}_y\text{-Pb}$, and $\text{W-W}_{x-y}\text{O}_y\text{-Sn}$ junctions. This enabled the determination of energy gap $\Delta(T)$ of W as function of temperature. The energy gap of W is found to obey the B.C.S. theory. Details on page A1-15 through A1-22.

1.4 Studies of Thermal Transpiration for the Development of a "Thermal Pump"

Senior Investigator: Dr. Manfred Altman

Graduate Student: E. Hopfinger

OBJECTIVE

To develop a gas pump without moving parts based on the thermal transpiration principle.

PREVIOUS ACCOMPLISHMENTS

- 1) Theoretical analysis of idealized system.
- 2) Experimental results of flow rates and steady state pressure differences as a function of mean pressure were reported, which are typical of thermal transpiration in membranes of finite thickness.
- 3) Thermal transpiration in membranes of finite thickness was formulated theoretically and the equations evolved reconciled with experimental results.

PROGRESS IN PAST PERIOD

Experiments have been extended to include five porous ceramics and two Millipore membranes of different geometric properties. An efficiency analysis was carried out and a merit factor defined in terms of physically meaningful quantities, such as thermal transpiration flow coefficient, isothermal permeability and apparent heat conductivity of the membrane material. A doctoral dissertation based on this work is under preparation. Details on page A1-23 through A1-30.

1.5 Thermoelectric Properties of Graphite Compounds

Principal Investigator - L. A. Girifalco

Graduate Students - S. Sachidanandam, T.M. DiVincenzo,
T. Montelbano

OBJECTIVE:

The objective of this work is to study the thermal and electronic properties of Graphite compounds with a view to ascertaining their possible value as thermoelectric materials. The work has proceeded along three lines: the preparation and characterization of a new compound, Barium-Graphite, a study of the electronic structure of layer structures, and a study of the lattice dynamics and phonon conductivity of Barium-Metal lamellar systems.

PREVIOUS ACCOMPLISHMENTS:

Barium-Graphite compounds were prepared, and theoretical studies were well under way. The three lines of work mentioned above are at a stage where a summary of each is in order. See page A1-31 through A1-37 for details.

N 68 - 2 1 0 3 9

2. PLASMA ENGINEERING

Branch Chief: Dr. Solomon Pollack

Senior Members: George Schrenk, Samuel Schweitzer, Hsuan Yeh

2.1 Flow of a Conducting Liquid in an Annular Gap: Experimental and Theoretical Study

I. M. Cohen

S. Schweitzer

T. Ebtekar

OBJECTIVES

To study the operation parameters and understand the flow in an electromagnetically driven mercury centrifuge or mercury rotor gyro.

PREVIOUS ACCOMPLISHMENTS

Magnetic field and pressure measurements have been made on our apparatus. The basic theoretical problems have been formulated.

PROGRESS IN PAST PERIOD

It has become apparent that because the electrode material is not perfectly conducting, certain idealizations are not valid. To look into this theoretically, we have solved the completely static three region (inner electrode, fluid, outer electrode) problem with finitely conducting electrodes. Corresponding potential measurements around the electrodes and in the fluid have been made.

We have started to look into the modes of secondary flow induced by the passage of current through the device (with no applied magnetic field). For small magnetic and fluid Reynolds numbers, an inhomogeneous biharmonic-like equation with homogeneous boundary conditions must be solved.

2.2 Basic Surface Investigations

G. L. Schrenk, S. Fonash, S. P. Sharma

Objectives

To study the influence of high fields on surface charge distributions on an atomic scale.

Previous Accomplishments

Research is in progress to understand the structure of field ion micrographs; in particular, we are trying to understand the varying average intensity of different regions and also the varying intensity of various dots. The regions of varying intensity are rather sharply defined and are more pronounced in some metals than in others - e.g., in platinum they form one of the most prominent features of the micrograph, while in tungsten they are barely discernible.

One possible explanation of these sharply defined regions is that they are related to the band structure of metals at their Fermi levels. We only need to consider the Fermi level because tunneling occurs only to the Fermi level of the metal at the low temperature and high field strengths involved.

Progress in Past Period

A quantum mechanical model of the tunneling process has been constructed and numerical results are being obtained for platinum. This model uses the actual structure of the Fermi surface of platinum. Preliminary results show that the shape of the Fermi surface does indeed influence the high field tunneling probability. Insufficient knowledge of the Fermi surface of platinum prevents us from making more than qualitative comparisons. This work is currently being written up and is the basis of Steve Fonash's Ph.D. dissertation.

Research on the varying intensity of the various individual dots,
rather than the zonal averages, has been started.

2.3 A Materials Study of Silicon Solar Cells

Senior Investigator: S. R. Pollack

Graduate Student: W. H. Becker

Objectives

This project is a detailed study of the effects of the basic materials properties of silicon solar cells upon their initial and long term performance.

Previous Accomplishments

None

Progress in Past Period

A literature search in the area of solar cell design and manufacture and the testing of solar cell materials (silicon, metals used in contacts, etc.) was begun. Preliminary samples of cells and cell assemblies were received from JPL and some reflectivity measurements have been made. Current work is being directed at the cell contact-solder-interconnection area.

N 68 - 21038

3. ELECTROCHEMICAL ENGINEERING

Branch Chief: Dr. Leonard Nanis

Senior Member: Dr. John O'M. Bockris

Postdoctoral Research Associate: Dr. Philippe Javet

3.1 Overpotential Transients on the Rotating Disk

Senior Investigator: Dr. L. Nanis

Graduate Student: Irving Klein

OBJECTIVE

The steady state voltage-time behavior for batteries under constant current drain has been used for many years in a purely empirical fashion (Peukert equation). Recent improved treatment based on a linear overpotential-current density relation does not fit results well as battery capacity (amp-hours) is diminished. The accelerated life testing of battery systems by cyclic charge-discharge schedules has, at present, no firm theoretical basis. The response of batteries to loads of variable depth of discharge may also be related through a theoretical treatment. The present problem is an attempt to treat in a rational way a typical battery electrode for which the mass transport is controlled to permit prediction of diffusional effects. The rotating disk geometry is ideal for this purpose and may be used in conjunction with actual battery electrodes and electrolytes. The present study will accomplish a long-desired treatment of combined activation and concentration overpotential transient behavior in order to focus attention on battery features such as changes in porous electrode structure, phase potential effects, and time effects due to defect structure in oxides and other battery materials. Engineering extension to fuel cells and batteries may be obtained by knowledge of local Nusselt numbers which control mass transport at working electrodes.

PREVIOUS ACCOMPLISHMENTS (new project)

PROGRESS IN PAST PERIOD

A mathematical model has been constructed for the transient redox overpotential decaying from steady state following interruption of galvanostatic conditions. The model includes initial conditions for the individual concentration profile of an oxidized and reduced species and the time

dependent . Navier-Stokes equation (or a rotating disk geometry). A functional relation between overpotential and concentrations has also been devised. A rotating disk system has been designed for experimental verification of the analytic treatment. See page A3-1 through A3-3 for details .

3.2 Current and Potential Distribution in Cylindrical Geometries: Engineering Application to Fuel Cell Design

Senior Investigator: Dr. L. Nanis

Graduate Student: Wallace Kesselman

OBJECTIVES

The mathematics of current distribution needed for fuel cell and battery design is complex principally because of boundary conditions in which potential gradient is a non-linear function of the local potential. Simplified one-dimensional models of porous electrodes necessarily omit features which fully describe the complex situation in which the mass transport of reactants and products of the electrode reaction is coupled with potential (and current density) distribution with further mutual interaction with the resulting thermal field. Correlations are needed to permit engineering evaluation of relative importance of flux terms under various conditions of electrode performance. The treatment of the three-dimensional configuration afforded by the cylindrical geometry will permit this special case to be fully evaluated for the dimensionless groups needed for correlation of electrode behavior and cell design, particularly on a scale corresponding to actual catalyst size.

PREVIOUS ACCOMPLISHMENTS

Two limiting cases of potential and current distribution have been represented analytically for a disk electrode, namely primary (constant potential) and uniform current distribution. These results have been applied to the simplification of membrane fuel cell design.

PROGRESS IN PAST PERIOD

An intermediate case of current distribution lying between primary and uniform has been solved for a linear relation between current density and

electrode overpotential. Previously encountered convergence difficulties were avoided by the use of singular integral equations. A functional relation was obtained between local current density and two dimensionless groups containing parameters of electrode size, electrolyte conductivity, electrode polarization and applied potential. This function displays the separation of polarization and position parameters for general applicability near to uniform current distribution. See page A3-4 through A3-8 for details.

3.3 Foaming Electrolyte Fuel Cell

Senior Investigator: Dr. L. Nanis

Research Specialist: A. P. Saunders

OBJECTIVES

The diffusion of reacting species provides an ultimate limitation in all electrochemical processes. For fuel cell applications, dissolved electroactive gases may be rapidly dissolved in a very thin film of electrolyte. Such a structure is provided by a foamed electrolyte and may be useful in practice if the rate of transport is sufficient and the circuit resistance is low. Verification of this possibility is the goal of present laboratory testing of cell geometries, surfactants and electrolytes.

PREVIOUS ACCOMPLISHMENTS

It has been demonstrated that electrode reaction can be supported through a foamed electrolyte. In studies on bright platinum, a new phenomenon was reported concerning alternation of potential near 0.7 V overpotential.

PROGRESS IN PAST PERIOD

Role of traces of oxygen in triggering the potential instability between the hydrogen reduction and oxygen evolution region has been determined by the use of helium gas purging in the cathode compartment. Extremely small rates of flow of hydrogen in foam were shown to reduce overpotential by as much as 0.4 V. The cause of this reduction is under study. For details see pages A3-9 through A3-12.

3.4 Atomic Scale Electrode Processes

P. Javet

L. Nanis

OBJECTIVES

The novel method combining field ion microscopy and electrochemistry, developed this contract, permits study of electrode surfaces with a resolution (3\AA) revealing the atomic phenomena which control the macroscopic behavior of fuel cell catalysts, battery materials and other types of electrodes. The virtual visualization of atomic processes, resulting from controlled electrochemical treatment aids the establishment of correct models for electrode kinetic behavior of utility in predicting macroscopic performance of practical electrodes.

PREVIOUS ACCOMPLISHMENTS

A systematic investigation of best conditions of image formation with different metals has shown that iridium is particularly well suited for our purposes. Results on evolution of gas on Ir. electrodes have been reported.

PROGRESS IN PAST PERIOD

The rearrangement of surface atoms induced on a F.I.M. tip by immersion into dilute Ir-ion solution (10^{-6}M) has been studied for a range of times (1 to 10 minutes). An initial rate of rearrangement of 2.5 layers per minute has been obtained. Details have been submitted for publication in Journal of the Electrochemical Society. See page A3-13 through A3-19.

3.5 PRIMARY AND SECONDARY CELLS USING CHARGE TRANSFER COMPLEXES

Senior Investigators: Dr. F. Gutman
A. P. Saunders

OBJECTIVES

To study and seek means to improve the performance of the Mg; Phenothiazine/I₂: C₂ or Pt system.

PREVIOUS ACCOMPLISHMENTS

Earlier work carried out elsewhere showed that the performance of this cell could be substantially improved when exposed to a high permittivity liquid or vapor such as water or Acetonitrile.

PROGRESS IN THE PAST PERIOD

Experiments have been made that show (a) Acetonitrile is not, as previously thought, and inert solvent to the Phenothiazine/Iodine complex. (b) The complex is the cathode in this system, the C₂ of Pt - being solely an electrical contact to the complex, the liquids or vapors being the electrolyte and (c) A new soft and ductile form of complex has been made. A novel technique for pressing powdered material into complex shapes is also described. For details see pages A3-20 through A3-26.

3.6 BOILING FUEL CELL

Senior Investigators: Dr. M. Altman
Dr. K. Sreenivasan
Advisor: Dr. Halina Wrobleva

OBJECTIVES:

Recent developments in high performance catalysts are rapidly revising activation polarization as the limiting resistance in fuel cells.

It is believed that nucleate boiling of an electrolyte could aid in the reduction of concentration polarization and facilitate heat removal.

The purpose of this study is to determine the feasibility and derivability of this mode of operation and to evaluate the advantages and penalties.

4. PUBLICATIONS LIST

Publications List

- INDEC-1 "The Optimization of MHD Generators with Arbitrary Conductivity", H. Yeh and T. K. Chu, ASME Paper 63-WA-349.
- INDEC-2 "The Prediction of Transient Heat Transfer Performance of Thermal Energy Storage Devices", M. Altman, D. P. Ross, H. Chang, Proceedings of 6th National Heat Transfer Conference, Boston, Mass., 1963.
- INDEC-3 "The Binary Eutectic as a Thermal Energy Storage System: Equilibrium Properties", G. R. Belton and Y. K. Rao, paper presented at the 6th National Heat Transfer Conference, Boston, Mass., August 11-14, 1963.
- INDEC-4 "Theoretical Model of a Thermionic Converter", J. Dunlop and G. Schrenk, Proceedings of Thermionic Specialist Conference, Gatlinburg, Tenn., pp. 57-62, Oct. 7-9, 1963.
- INDEC-5 "Thermophysical and Transport Properties of High Temperature Energy Storage Materials", R. Sharma and H. Chang, paper presented at the Third Annual Symposium, High Temperature Conversion Heat to Electricity, Tucson, Arizona, Feb. 19-21, 1964.
- INDEC-6 "Solar Collection Limitations for Dynamic Converters-Simulation of Solar-Thermal Energy Conversion Systems", G. L. Schrenk, Proceedings of AGARD Conference, Cannes, France, March 16-20, 1964.
- INDEC-7 "Prospects for Thermal Energy Storage", M. Altman, Proceedings of AGARD Conference, Cannes, France, March 16-20, 1964.

- INDEC-8 "The Hollow Thermionic Converter", L. Zelby, IEEE
Annual Meeting on Energy Conversion, Clearwater,
Florida, May, 1964.
- INDEC-9 "The Institute for Direct Energy Conversion", M. Altman,
paper presented at AM. Soc. Eng. Ed. Annual Meeting,
University of Maine, Orono, Maine, June 22-26, 1964.
- INDEC-10 "Emitter Sheath Polarity in Plasma Diodes", G. Schrenk,
Proceedings of Thermionic Specialist Conference,
Cleveland, Ohio, Oct. 26-28, 1964, pp. 249-257.
- INDEC-11 "Electron Emission from Metals in Gaseous Environment",
M. Kaplit, G. Schrenk, L. Zelby, Proceedings of Thermionic
Specialist Conference, Cleveland, Ohio, Oct. 26-28, 1964,
pp. 4-10.
- INDEC-12 "Criteria for Emitter Sheath Polarity in Plasma Diodes",
G. Schrenk, paper presented at ASME Winter Annual Meet-
ing, New York, No. 29, Dec. 3, 1964.
- INDEC-13 "An Electrochemical and Microbiological Study of the
Formic Acid-Formic Dehydrogenlyase System", R. J. Blasco
and E. Gileadi, Advanced Energy Conversion, Vol. 4,
pp. 179-186, 1964.
- INDEC-14 "Mathematical Simulation of Solar Thermionic Energy Con-
version Systems", G. Schrenk and A. Lowi, Proceedings of
the International Thermionic Electrical Power Generation
Conference, IEEE, London, England, Sept. 20-24, 1965.
- INDEC-15 "Cavity Receiver Temperature Analysis", R. McKinnon,
A. Turrin, G. Schrenk, AIAA paper No. 65-470, July 26-29,
1965.

- INDEC-16 "Electron Emission from Metals in Vapors of Cesium and Fluorine", G. Schrenk and M. Kaplit. Proceedings of the Thermionic Specialist Conference, San Diego, California, October 25-27, 1965.
- INDEC-17 "Longitudinal Interaction of Microwaves with an Argon Discharge", C. A. Renton and L. W. Zelby, Appl. Phys. Ltrs., Vol. 6, No. 8, pp. 167-169, September 15, 1965.
- INDEC-18 "Microwave Interaction with a Non-Uniform Argon Discharge", L. W. Zelby, Proceedings of the Symposium of Microwave Interaction with Ferrimagnetics and Plasmas, London, England, pp. 32-1 to 32-3, September 13-17, 1965.
- INDEC-19 "Two-Phase Flow and Heat Transfer for Boiling Liquid Nitrogen in Horizontal Tubes", M. Altman and J. H. Jones, Chemical Engineering Progress Symposium Series, Volume 61, No. 57, October, 1965.
- INDEC-20 "Electrical Conductivity of a Partially Ionized Gas in a Magnetic Field", S. Schweitzer and M. Mitchner. Physics of Fluids, 10, 799-806 (1967).
- INDEC-21 "Models for Electron Emission from Metals with Adsorbed Monolayers", M. Kaplit, G. L. Schrenk, and L. Zelby. Advanced Energy Conversion, Vol. 7, pp. 177-189, 1967.
- INDEC-22 "Models for Electron Emission from Metals with Adsorbed Monolayers", M. Kaplit and G. L. Schrenk. Proceedings of the Twenty-Sixth Annual Conference on Physical Electronics, Massachusetts Institute of Technology, Cambridge, Mass., March 21-23, 1966.

- INDEC-23 "Slow Wave Interaction with an Argon Discharge", (Abstract)
L. W. Zelby, Symposium on Properties and Applications of
Low-Temperature Plasmas, XX-th International Congress of
I.V.P.A.C., Moscow, USSR, July 15-18, 1965.
- INDEC-24 "Understanding Plasma Diodes and Amplifiers", L. W. Zelby,
Electronic Industries, Vol. 24, No. 11, p. 64, Nov. 1965.
- INDEC-25 "A Simplified Approach to the Analysis of Electromagnetic Wave
Propagation Characteristics of Plasma Coated Surfaces",
L. W. Zelby, RCA Review, Vol. 26, No. 4, p. 497, Dec. 1965.
- INDEC-26 "Plasma Coated Surface as a Wave Guide", L. W. Zelby,
RCA Engineer, Vol. 11, No. 4, p. 50, January 19, 1966.
- INDEC-27 "Measurements of Collision Frequency in an Argon Discharge",
L. W. Zelby, W. O. Mehuron, R. Kalagher, Applied Physics
Letters, June 15, 1966, Vol. 21, No. 5, pp. 522-524.
- INDEC-28 "Effects of Inhomogeneous Electron Density in a Cylindrical
Plasma Column Surrounded by a Helix", R. Kalagher,
Submitted to IEEE Transactions on Microwave Theory and
Techniques, March 1966.
- INDEC-29 "Syringe for Injecting Sodium Potassium Alloy", Samuel
Greenhalgh, The Review of Scientific Instruments, Vol. 38,
No. 1, pp. 121-122, January 1967.
- INDEC-30 "Characteristics of Plasma Probes in a MHD Working Fluid",
A. Whitman, H. Yeh. Proceedings of International Symposium
on Magnetohydrodynamic Electrical Power Generation, Salzburg,
Austria, July 4-8, 1966, International Atomic Energy Agency,
pp. 127-144.

- INDEC-31 "Convergence of Successive Approximations to the Scalar Electrical Conductivity of Some Weakly Ionized Real Gases", S. Schweitzer, M. Mitchner, published in the A.I.A.A. Journal, Volume 5, No. 2, pp. 351-353, 1967.
- INDEC-32 "The Determination of Thermal Diffusivities of Thermal Energy Storage Materials, Part 1, Solids Up To Melting Point", Han Chang, Manfred Altman, Ram Sharma. Published in the A.S.M.E. Journal, Vol. 89, Series A, #3, pp. 407-414, July, 1967.
- INDEC-33 "Electrochemical Principles of Corrosion", Leonard Nanis, presented at the National Association of Corrosion Engineers Symposium, September, 1966, Philadelphia, Penna.
- INDEC-34 "Tolerance Specification by Multiple Alignment Statistics", L. Nanis, presented at Session 14, "Effective Utilization of Grid-Based Interconnection Systems", proceedings of the 1966 Western Electronic Show and Convention, Los Angeles, California, August, I.E.E.E.
- INDEC-35 "The Tensor Electrical Conductivity of Atmospheric Cesium-Seeded Argon", S. Schweitzer, A.I.A.A. Journal, Volume 5, No. 5, pp. 844-846 (1967).
- INDEC-36 "The Reaction of Molten Metal Droplets with a Rarefield Atmosphere", by M. Altman, D. Ross. Published in the A.I.A.A. Journal, April 1967, Vol. 5, No. 4.
- INDEC-37 "Electron Transfer Processes Through Tantalum-Tantalum Oxide Diodes", S. Pollack. Journal of Applied Physics, November, 1966.

- INDEC-38 "A Method for Determination of the Permeation Rate of Hydrogen Through Metal Membranes", J. McBreen, W. Beck, L. Nanis, Journal of Electrochemical Society, 113, No. 11, pp. 1218-1222 (November 1966).
- INDEC-39 "Tensor Electrical Conductivity of a Partially Ionized Gas in a Magnetic Field", S. Schweitzer and M. Mitchner. Physics of Fluids, 10, 799-806 (1967).
- INDEC-40 "New Method of Producing Electric Power by Means of a Thermionic Converter". Patent application by M. Altman.
- INDEC-41 "A Metal-Oxide Thin Film Photovoltaic Energy Converter". Patent application by M. Altman and S. R. Pollack.
- INDEC-42 "Current & Potential Distribution in Cylindrical Geometries: Engineering Applications", L. Nanis, submitted to Journal Electrochemical Society. Presented at Current Distribution Symposium, Dallas, May 1967 Meeting, Electrochemical Society.
- INDEC-43 "Overpotential-Time Variation for Galvanostatic Charging with Potential Dependent Capacitance", L. Nanis, P. Javet. Journal of The Electrochemical Society, Vol. 114, No. 8, August, 1967.
- INDEC-44 "Galvanostatic Charging with Potential Dependent Double Layer Capacitance", L. Nanis, P. Javet, to be submitted to Electrochimica Acta.
- INDEC-45 "Decay of Overpotential from the Tafel Region with Potential Dependent Double Layer Capacitance", L. Nanis, P. Javet, to be submitted to Journal of Electrochemical Society.

- INDEC-46 "Status of Magnetohydrodynamic Power Generation for Terrestrial Applications", H. Yeh, presented at the A.I.A.A. Third Annual Meeting in Boston, Massachusetts, Nov. 29 - Dec. 2, 1966. A.I.A.A. Paper 66-1013.
- INDEC-47 "First Order Effects of Production on the Continuum Theory of Spherical Electrostatic Probes", Ira M. Cohen and S. Schweitzer. Published in the A.I.A.A. Journal, Vol. 6, No. 2, pp. 298 - 304, February, 1968.
- INDEC-48 "The Electric Automobile - A Discussion of Strategy, Tactics, and Leadership", M. Altman, presented at the National Electric Automobile Symposium, San Jose, California, February 24, 25, 1967.
- INDEC-49 "The Electric Automobile - Its Future", M. Altman, presented at the IEEE International Convention, New York, March 20 - 23, 1967.
- INDEC-50 "A Method of Accelerating the MRD Method When Sharp Ridges are Present", F. A. Costello and G. L. Schrenk. Submitted to J. Comp. Physics.
- INDEC-51 "Numerical Solution to the Heat Transfer Equation with Combined Conduction & Radiation", F. A. Costello and G. L. Schrenk. Submitted to J. Comp. Physics.
- INDEC-52 "The Optimization of Space-Craft Coating Patterns for Temperature Control", F. A. Costello, T. P. Harper, R. Kidwell, and G. L. Schrenk. Submitted to the forthcoming ASME Heat Transfer Conference.
- INDEC-53 "Flow of a Conducting Liquid in an Annular Gap: A Restricted Nonexistence Proof", S. Schweitzer and I. M. Cohen. A.I.A.A. Journal, Vol. 5, No. 11, pp. 2066-2068.

- INDEC-54 "The Determination of Thermal Diffusivities of Thermal Energy Storage Materials, Part II: Molten Salts Beyond the Melting Point", K. Sreenivasan, M. Altman. To be published in ASME Journal of Power.
- INDEC-55 "Temperature Measurement of an Alkali Metal-Seeded Plasma in an Electric Field", T. K. Chu and Chad F. Gottschlich. Published in the A.I.A.A. Journal, Vol. 6, No. 1, pp. 114 - 119, January, 1968.
- INDEC-56 "On the Accuracy of Calculating the Scalar Electrical Conductivity at Very Low Ionization Levels", S. Schweitzer. Published in the A.I.A.A. Journal, Vol. 5, No. 11, pp. 2086 - 2087.
- INDEC-57 "Investigations on Seeded Cesium Plasma Diodes", A. Kaufman and G. Schrenk, Proceedings of the Thermionic Specialist Conference, Palo Alto, California, Oct. 30-Nov. 1, 1967.
- INDEC-58 "Seeded Cesium Plasma Diodes and the Penning Effect", A. Kaufman and G. L. Schrenk. Submitted to Journal of Applied Physics.

MATERIALS ENGINEERING

APPENDIX

A-1

Thermal Diffusivity of Liquids

Senior Investigator: Dr. Manfred Altman

Post-doctoral Fellow; Dr. K. Sreenivasan

The theory and the experimental details of the method have been described in previous reports. Fundamentally, the difference between the temperature at the surface and at the center of a cylindrical container is measured for a constant rate of surface temperature rise. The liquid, whose thermal diffusivity is to be measured, is contained in an annular groove concentric with the surface. Note that it is not necessary to measure the temperature of the liquid. The width of the groove is so small as to maintain "creeping thermal motion" in the liquid. This minimizes free convection effects to a negligible value.

The thermal diffusivity of the container material is essential for calculating liquid thermal diffusivity. This report presents the experimental results for the thermal diffusivity of the container material. The experimental technique is similar to the one described above with this difference--the cylindrical container is replaced by a solid cylindrical specimen. The material of the specimen is boron nitride. The surface temperature and the difference between the surface temperature and the temperature at the center are monitored in separate recorders. The thermal diffusivity of the specimen is calculated using the recorder data. The experimental results are presented in Fig. 1.

A new 2 3/8" Dia. Pt - 40% Rh wire-wound-furnace has been designed and built. This was used for the liquid diffusivity measure-

ments. The results are presented in the next section.

Experimental Results

It was decided to calibrate liquid-diffusivity cell by testing a liquid whose thermal diffusivity has been measured by other investigators. Sodium nitrate (melting point 306.8°C) was chosen as the liquid. Sodium nitrate was tested in the 0.0625 inch annular gap container. The results are shown in Fig. 2. As seen in this figure, the results of this investigation compare very favorably with the results of Bloom et al (Ref. 1).

Lithium fluoride liquid was tested in two containers whose gap widths were different, in order to detect the influence of free convection. It may be recalled that the influence of free convection is proportional to the cube of the gap width. The results obtained with both the containers are shown in Fig. 3. No discernible difference exists in these results. It is reasonable to conclude that free convection effects are negligibly small. The functional relation between the thermal diffusivity of liquid LIF and temperature was obtained by the method of least squares. It is given by

$$\alpha_{LIF} = 0.0152 + 10^{-6} \times T$$

where

$$\alpha_{LIF} - \text{ft}^2/\text{hour} \quad \& \quad T \text{ in } ^{\circ}\text{C}$$

The straight line drawn in Fig. 3 satisfies the above relation. The average deviation of the experimental points from this line is 1.60%, with a minimum of 0.06% and a maximum of 6.93%.

The thermal conductivity of lithium fluoride in the solid and the liquid state is shown in Fig. 4. The thermal conductivity ratio in the

two states k_L/k_S is found to be equal to $1.0/3.0=0.66$ (the extrapolated value at the melting point is used for the solid). Turnbull (Ref. 2), using the derivation of Keyes (Ref. 3), calculates a value of 0.79 for the ratio of k_L/k_S for ionic solids. Turnbull's (Ref. 2) own analysis of the following liquids - NaNO_3 , KNO_3 , NaCl , AgNO_3 , KHSO_4 , NaHSO_4 , NH_4HSO_4 , KCNS , ZnCl_2 and NaOH gave a value of k_L/k_S in the range 0.71 to 0.99. The value of $k_L/k_S = 0.66$ obtained in this investigation compares favorably with the values reported in the literature.

Semi-theoretical expressions for the thermal conductivity of molten salts have been compiled by Gambill (Ref. 4). The correlations suggested are in terms of the density, molecular weight and the melting point of the molten salt.

$$k = 1.21 T_m^{1/2} \rho_m^{2/3} M^{-7/6} \quad (1)$$

$$k = 0.75 T_m^{1/2} \rho_m^{2/3} M^{-7/6} \quad (2)$$

For lithium fluoride

$$T_m = 1143^\circ\text{K}$$

$$\rho_m = 1.8 \text{ gms/cm}^3$$

$$M = 25.94$$

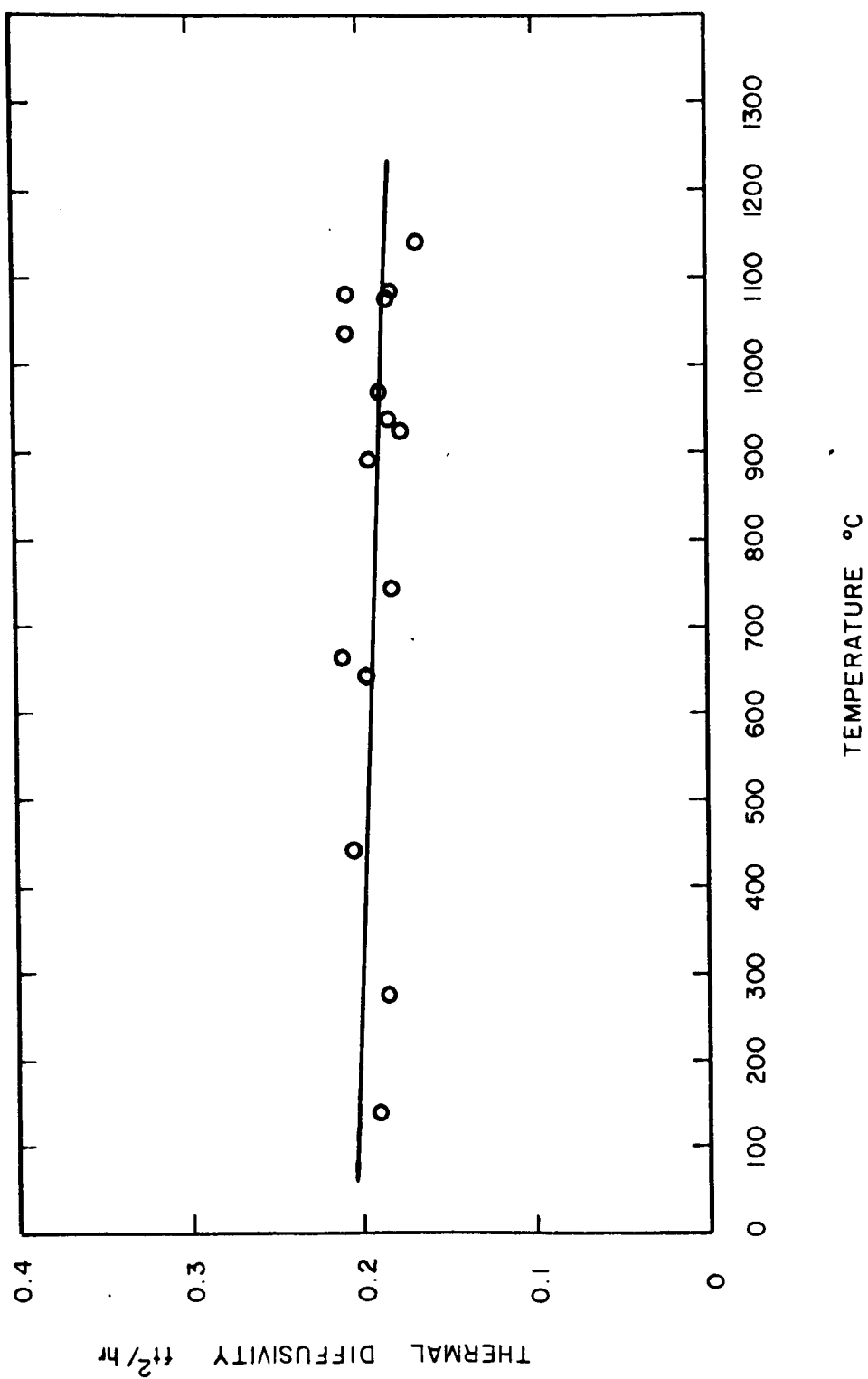
Using these values, equation (1) gives a value of $k = 1.36 \text{ BTU/hr ft F}$; equation (2) gives a value of $k = 0.85 \text{ BTU/hr ft F}$. The measured value of k is 1.0 BTU/hr ft F . By using a constant of 0.9 instead of either 1.21 or 0.75, the thermal conductivity experimentally measured in this

investigation can be correlated with its melting point, density and molecular weight. The correlating equation then becomes

$$k = 0.9 T_m^{1/2} \rho_m^{2/3} M^{-7/6}$$

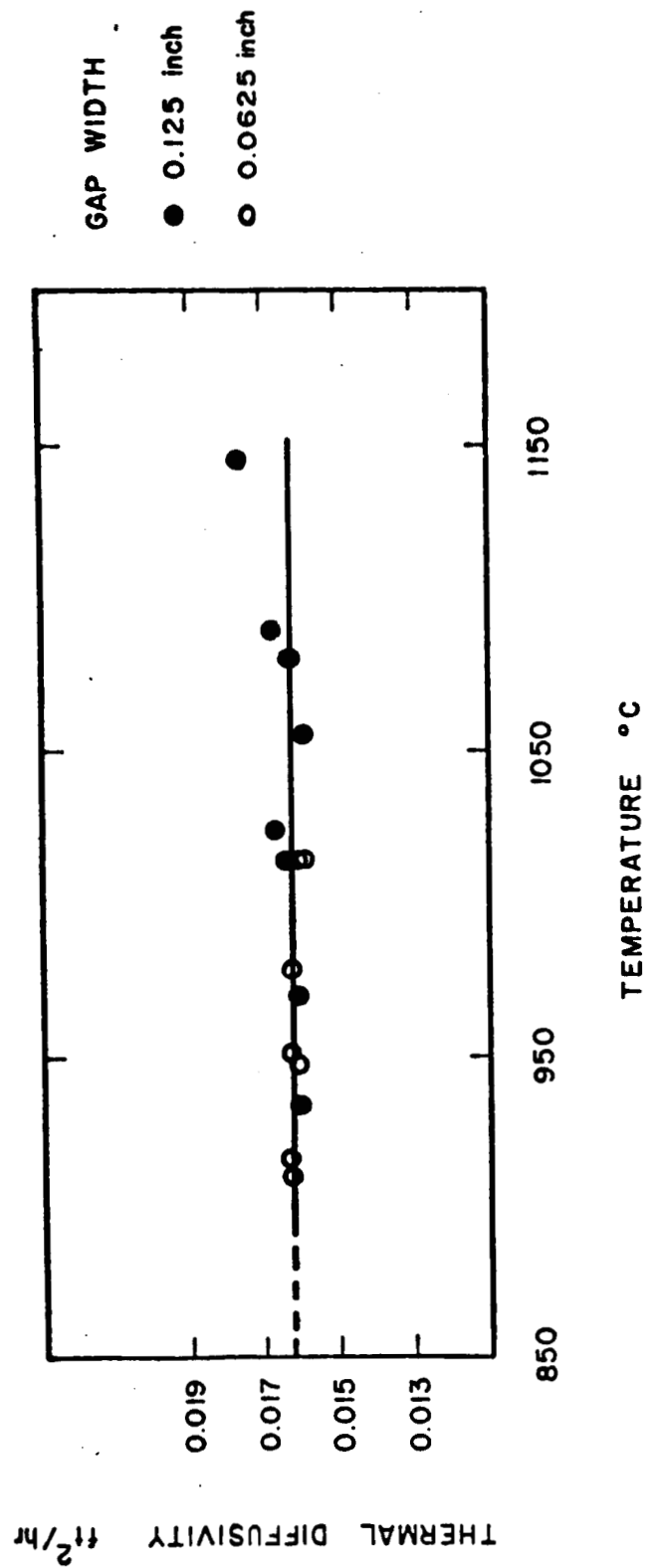
REFERENCES

1. H. Bloom, A. Doroszkowski and S. B. Tricklebank:
"Molten Salt Mixtures, IX, The Thermal Conductivity of Molten Nitrate Systems!" Australian Journal of Chemistry, 18, 1171-6, 1965.
2. A. G. Turnbull : "The Thermal Conductivity of Molten Salts, II. Theory and Results for Pure Salts," Australian Journal of Applied Science, 12, 324-9, 1961.
3. R. W. Keyes: "High Temperature Thermal Conductivity of Insulating Crystals: Relationship to the Melting Point!" Physical Reviews, 115, 564-7, 1959.
4. W. R. Gambill: "Fused Salt Thermal Conductivity," Chemical Engineering, 12, 129-130, August 1959.
5. K. Sreenivasan: "A Quasi-steady Method for Measuring the Thermal Diffusivity of Molten Salts!" Ph. D dissertation, University of Pennsylvania, December 1967.



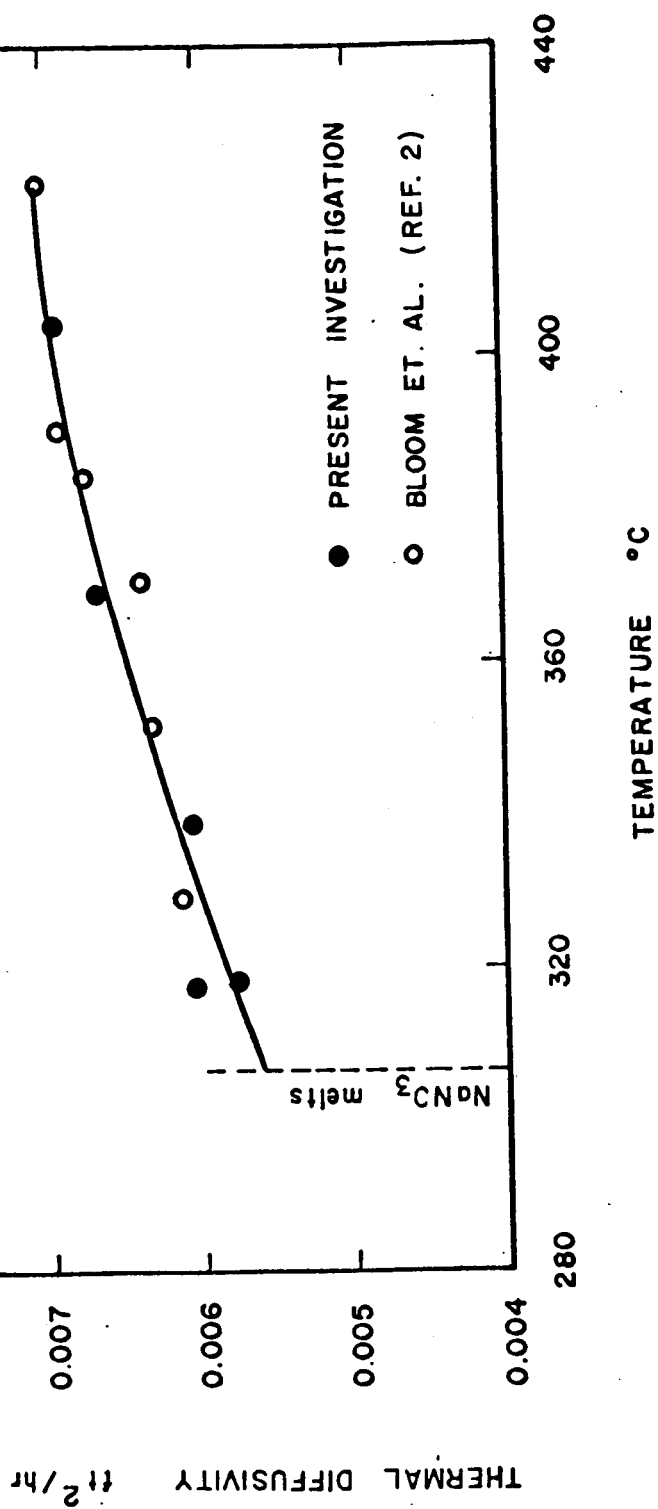
THERMAL DIFFUSIVITY OF BORON NITRIDE

FIG. 1



Thermal Diffusivity of Lithium Fluoride

FIG. 3



Thermal Diffusivity of Sodium Nitrate

FIG. 2

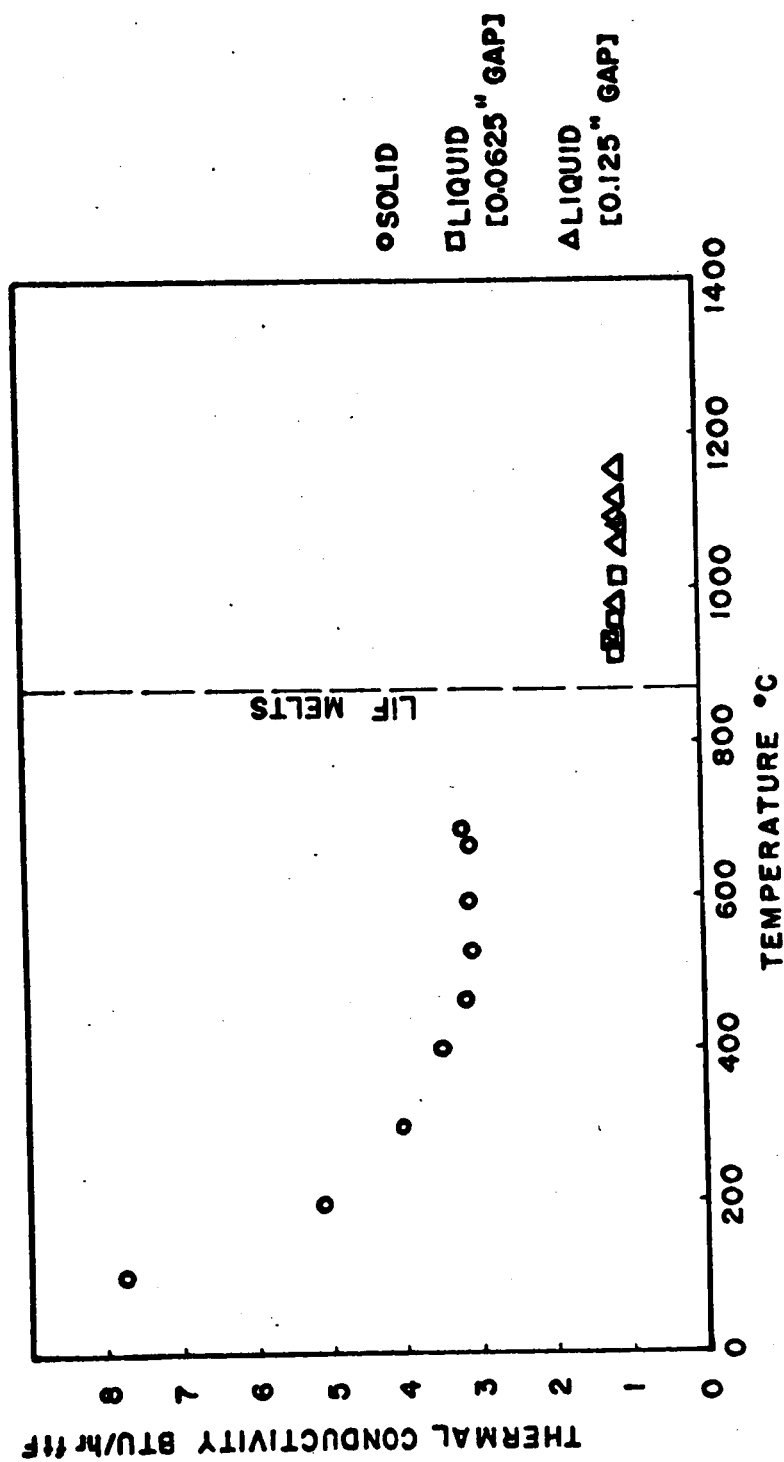
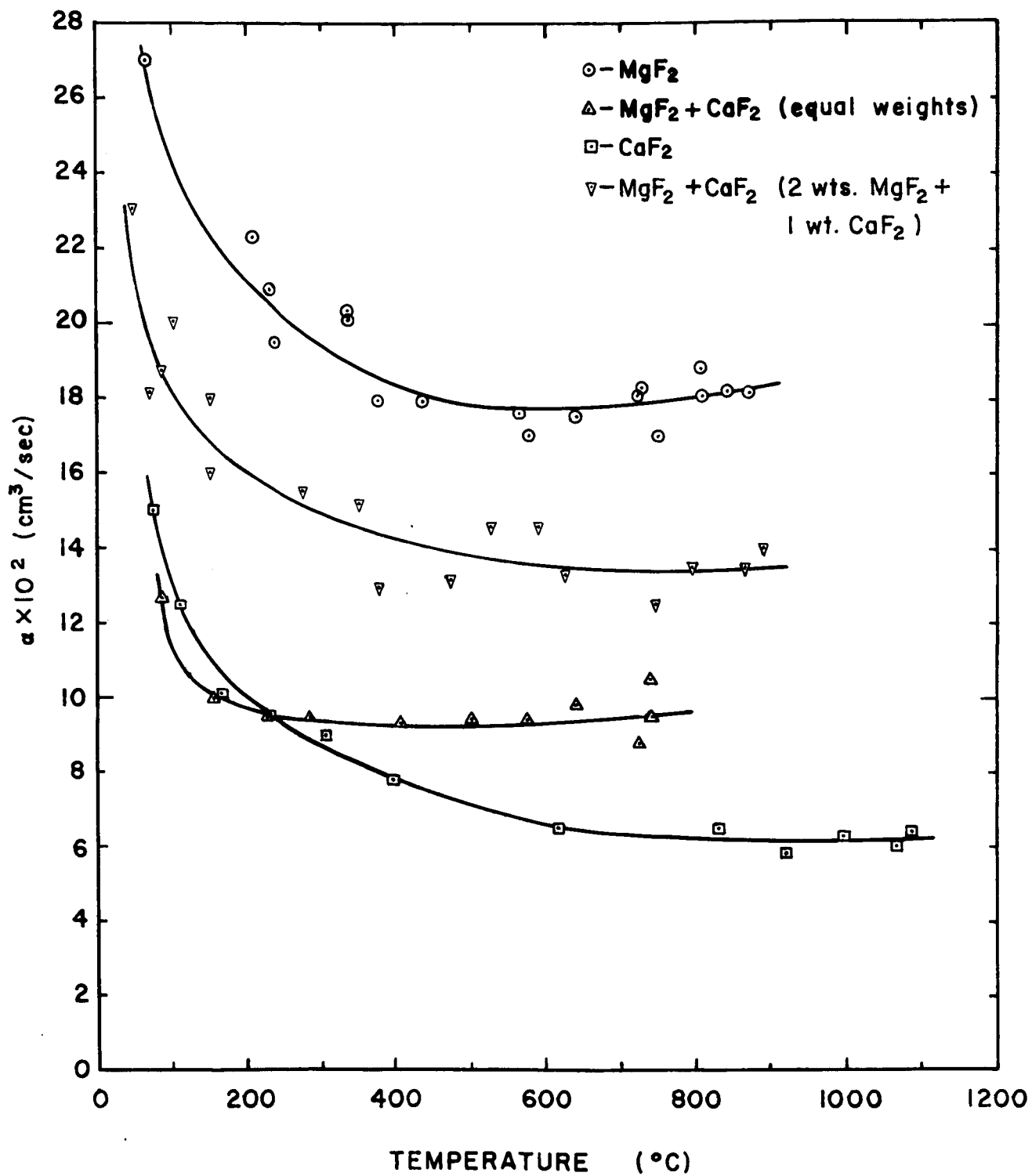


FIG. 4 - THERMAL CONDUCTIVITY OF LITHIUM FLUORIDE



THERMAL DIFFUSIVITY OF CaF_2 , MgF_2 , AND THEIR MIXTURE

FIG. 1

TABLE 1

Thermal Diffusivity of CaF_2 , MgF_2 and Their
Mixtures

Temp. (°C)	CaF_2	MgF_2	$\frac{1}{2} \text{MgF}_2 + \frac{1}{2} \text{CaF}_2$	$\frac{2}{3} \text{MgF}_2 + \frac{1}{3} \text{CaF}_2$
100	12.9	24.2	11.6	18.3
200	9.9	21.3	9.9	16.0
300	8.75	19.3	9.5	14.9
400	7.8	18.2	9.3	14.3
500	7.3	17.9	9.25	13.9
600	6.8	17.75	9.30	13.6
800	6.2	18.1	9.60	13.4
900	6.1	18.4	---	13.5
1000	6.13	---	---	---
1100	6.3	---	---	---

TABLE I

	Cu Cd ₂ In Te ₄	Cu Zn ₂ In Se ₄
Lattice parameter	6.34 Å	6.15 Å
Axial ratio	2.00	2.00
Thermoelectric power @ 300°K	215 μv/°K	154 μv/°K
Electrical resistivity @ 300°K	6.35 x 10 ⁻² ohm-cm	3.84 x 10 ⁻¹ ohm-cm
Conductivity type	p	p
Carrier density @ 300°K	2.36 x 10 ¹⁹ /cc	4.92 x 10 ¹⁸ /cc
Carrier mobility @ 300°K	4.16 cm ² /volt-sec	3.31 cm ² /volt-sec
Temperature dependence of mobility	~ T ^{+0.5}	~ T ^{-0.6}
Knoop microhardness	149 KHN	189 KHN

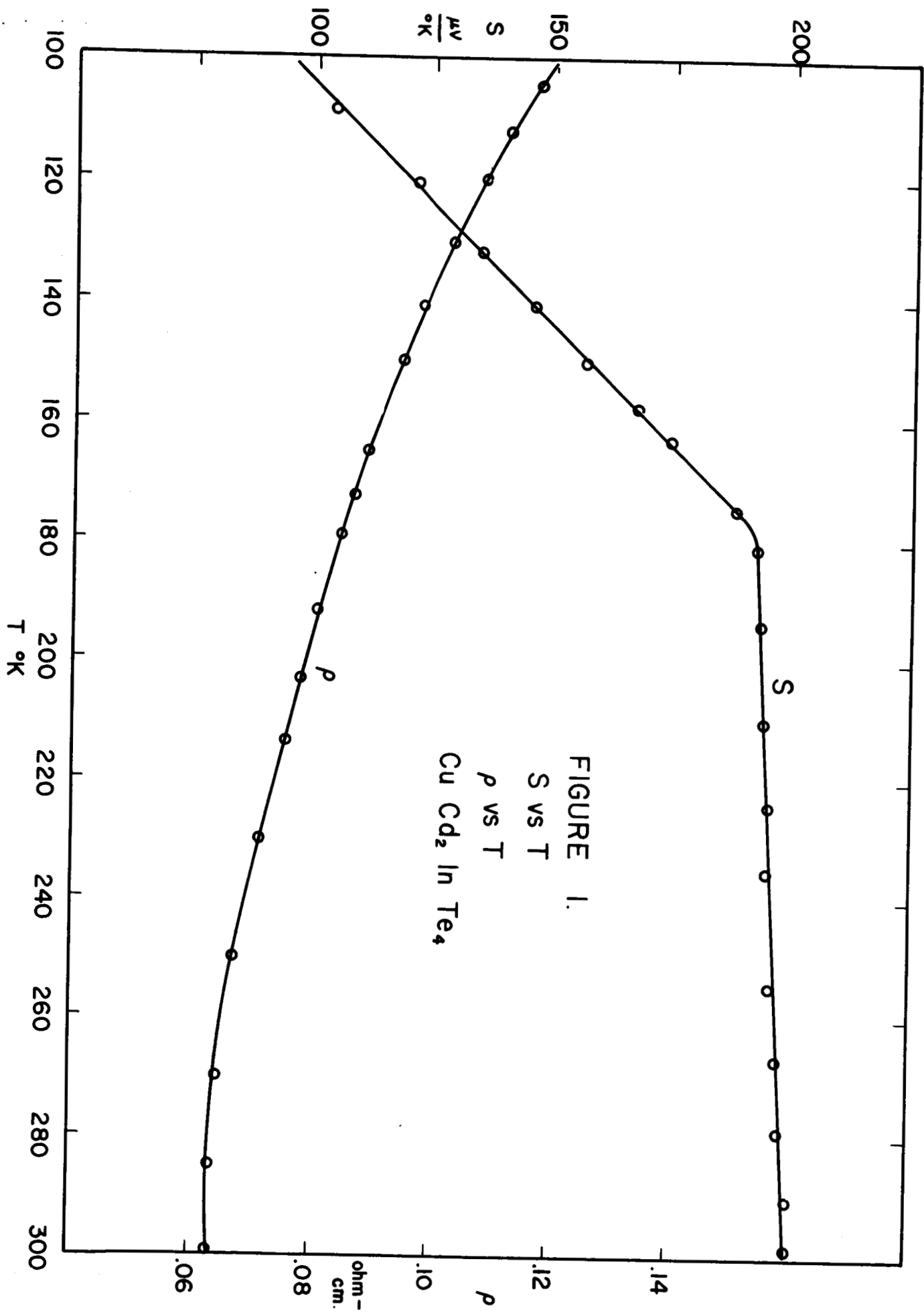
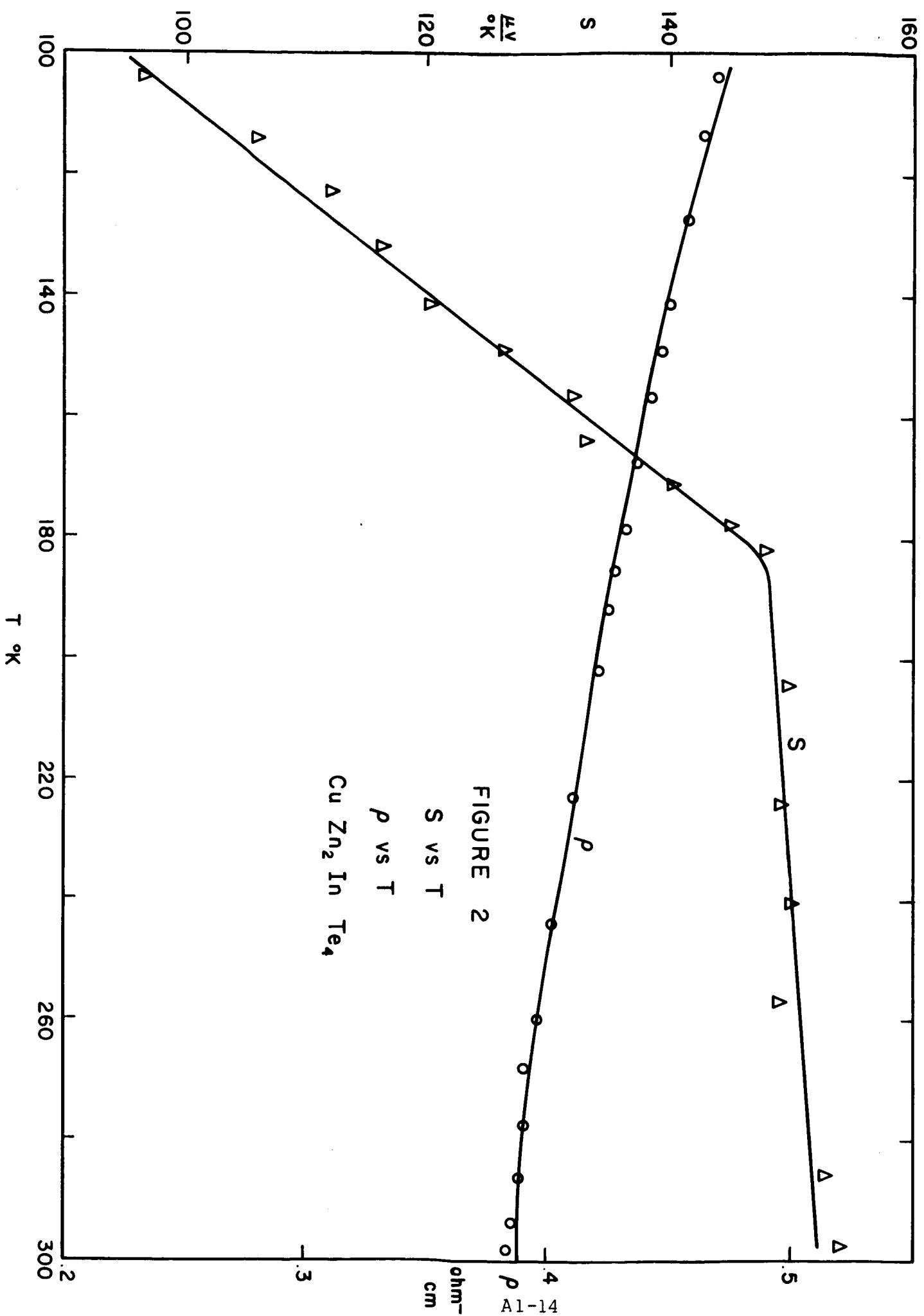


FIGURE 1.
S vs T
 ρ vs T
 $\text{CuCd}_2\text{InTe}_4$



SUPERCONDUCTIVITY IN EVAPORATED TUNGSTEN FILMS*

S. Basavaiah and S. R. Pollack

School of Metallurgy and Materials Science,
University of Pennsylvania,
Philadelphia, Pennsylvania.

Recently there have appeared several papers¹⁻⁴ dealing with the structure and microstructure of tungsten thin films and the relationship of structure to the occurrence of superconductivity. Common to all these papers is the result that W films have high superconducting transition temperatures, T_c , compared to the bulk values,¹⁻³ the enhancement in T_c being as large as a factor of 400. Kammerer and Strongin^{1,2} have suggested that the small particle size commonly found in evaporated refractory metals correlates with the T_c enhancement, while Bond et al.³ detected the presence of the β -W (A15) phase in their samples. Chopra et al.⁴ have detected an FCC phase in sputtered W films. It is the purpose of this letter to show that the β -W phase is present, that its presence is most likely stabilized by oxygen during the vacuum deposition, and that the superconducting energy gap in the β -tungsten is adequately described by BCS theory.

Samples were prepared by electron beam evaporating MRC triple zone-refined tungsten onto 7059 Corning glass substrates in a bakeable ultra high vacuum system. A number of films were prepared

at pressures of 3×10^{-6} , 2×10^{-7} , and 3×10^{-9} torr, where the pressures are measured near the substrate during evaporation. Evaporation rates varied from 20 to $47 \text{ \AA}/\text{min}$. and film thickness varied from 500 to 1500 \AA . The results reported here did not vary significantly with these evaporation rates or thicknesses. The resistivity of the films was approximately $10^{-4} \Omega\text{-cm}$. The structure of the films was studied by both x-ray and electron diffraction. Figures 1 and 2 show typical diffraction data for samples made at the upper and lower extremes of pressure. In all cases samples prepared at 10^{-6} torr were superconducting above 3°K and showed the presence of the β -W phase.

It is evident from these figures that for evaporation pressure of 10^{-6} torr, both x-ray and electron diffraction confirm the presence of β -W. As the pressure is decreased the (200) and (211) lines of the β -W phase decrease in intensity and the (110) α -W line increased in intensity until at 10^{-9} torr only α -W (BCC) remains. Superconducting transition temperatures were measured for these samples and an average $T_c = 3.2^\circ\text{K}$ was obtained for samples made 10^{-6} torr in agreement with Bond et al.³ As the pressure during evaporation is decreased, T_c decreases such that for 10^{-9} torr samples we could not detect superconductivity down to 1.0°K . This is expected since T_c for α -W is only 0.01°K .⁵ We suggest therefore that the T_c enhancement in vacuum deposited W films is due to the presence of the β -W phase in

agreement with Bond et al.³ and that this phase is stabilized⁶ by the presence of oxygen in the vacuum system during deposition.

These results further indicate that both α -W and β -W phases are present when the pressure during evaporation is between 10^{-6} torr and 10^{-9} torr (for our evaporation rates; the pressure range may of course be different for different evaporation rates). Therefore we suggest that the variability of T_c from one sample to another, and the decrease in T_c with pressure during evaporation is related to the connectivity of the β -W regions, a particle size effect in the β -W regions or both. The effect of oxygen on the structure of tungsten films was suggested by Kammerer and Strongin,² and although they were unable to observe it, this work confirms their hypothesis.

Tunnel junctions were prepared on samples made at 10^{-6} torr using Pb and Sn counterelectrodes. In this way the energy gap was determined as a function of temperature using standard techniques⁷ and the results are shown in Fig. 3. Excellent agreement with the BCS⁸ theory is evident. This represents the first reported energy gap measurements for β -tungsten.

The helpful discussions with Drs. K. L. Chopra, A. Dahm, A. Jensen, J. R. Schreiffer, and W. Worrell are gratefully acknowledged.

*Sponsored by Institute for Direct Energy Conversion, University of Pennsylvania.

REFERENCES

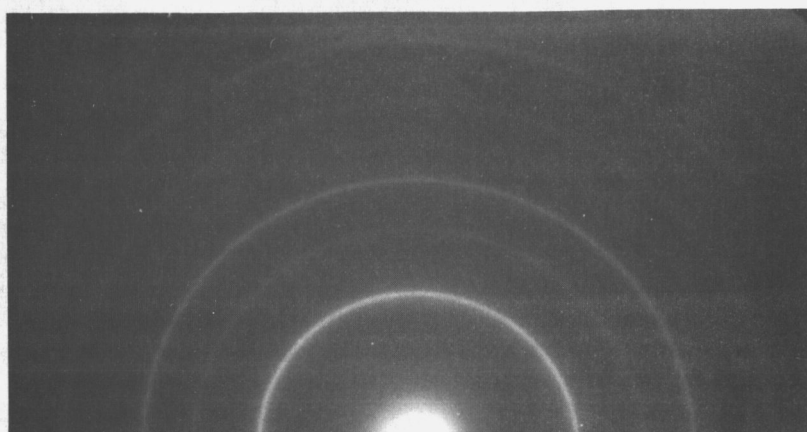
1. O. F. Kammerer, and M. Strongin, Phys. Letters, 17, 224 (1965)
2. O. F. Kammerer and M. Strongin, Proc. of the Inter. Symp. held at Clausthal-Göttingen, Sept. 1965.
3. W. L. Bond, A. S. Cooper, K. Andres, G. W. Hull, T. H. Gaballe, and B. T. Matthias, Phys. Rev. Letters, 15, 260 (1965).
4. K. L. Chopra, M. R. Randle and R. H. Duff, Appl. Phys. Letters, 9, 402 (1966).
5. J. W. Gibson and R. A. Hein, Phys. Rev. Letters, 12, 688 (1964).
6. H. I. Kaplan and W. L. Worrell, Trans. Met. Soc., AIME (1968) (To be published).
7. I. Giaever and K. Megerle, Phys. Rev., 122, 1101 (1961); B. N. Taylor, Ph.D. dissertation, University of Pennsylvania, 1963.
8. J. Bardeen, L. N. Cooper and J. R. Schrieffer, Phys. Rev., 108, 1175 (1957).

FIGURE CAPTIONS

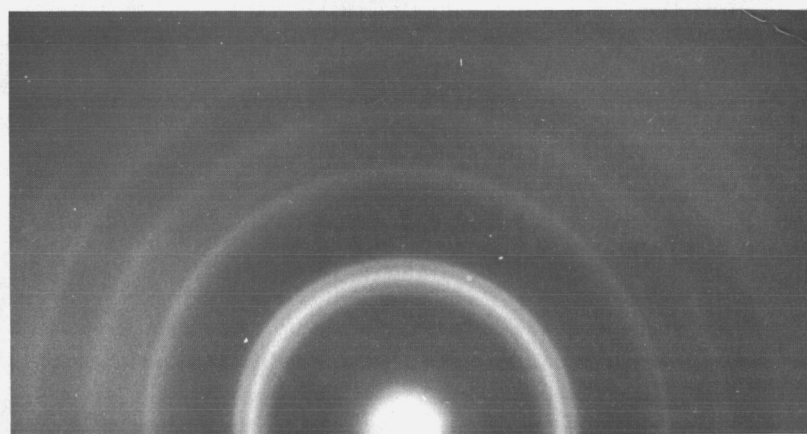
Figure 1. X-ray diffraction pattern for W films, with pressures during deposition of (a) 3×10^{-9} torr. (b) 2×10^{-6} torr.

Figure 2. Electron diffraction pattern for α and β W films.

Figure 3. Energy gap $\Delta(T)$ of β -W as a function of temperature T. T_c varied from 3.1°K to 3.3°K and the corresponding value of $2\Delta(0)/KT_c$ are 2.63 and 3.64 respectively.



(a) 3×10^{-9} torr.



(b) 2×10^{-6} torr.

FIGURE 1

X-ray diffraction pattern for W films
with pressures during deposition of

(a) 3×10^{-9} torr.

(b) 2×10^{-6} torr.

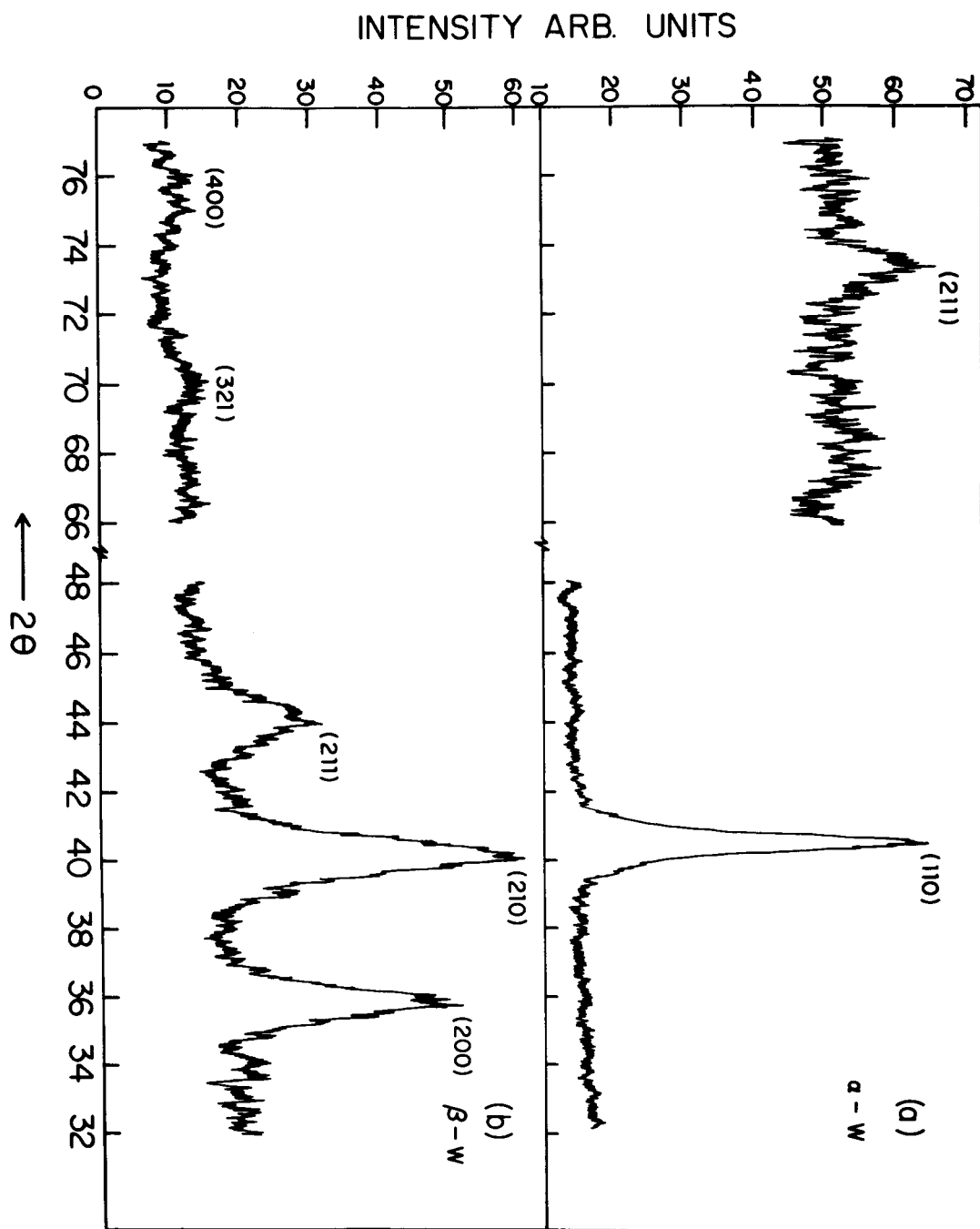


FIGURE 2

Electron diffraction pattern for α and β W films.

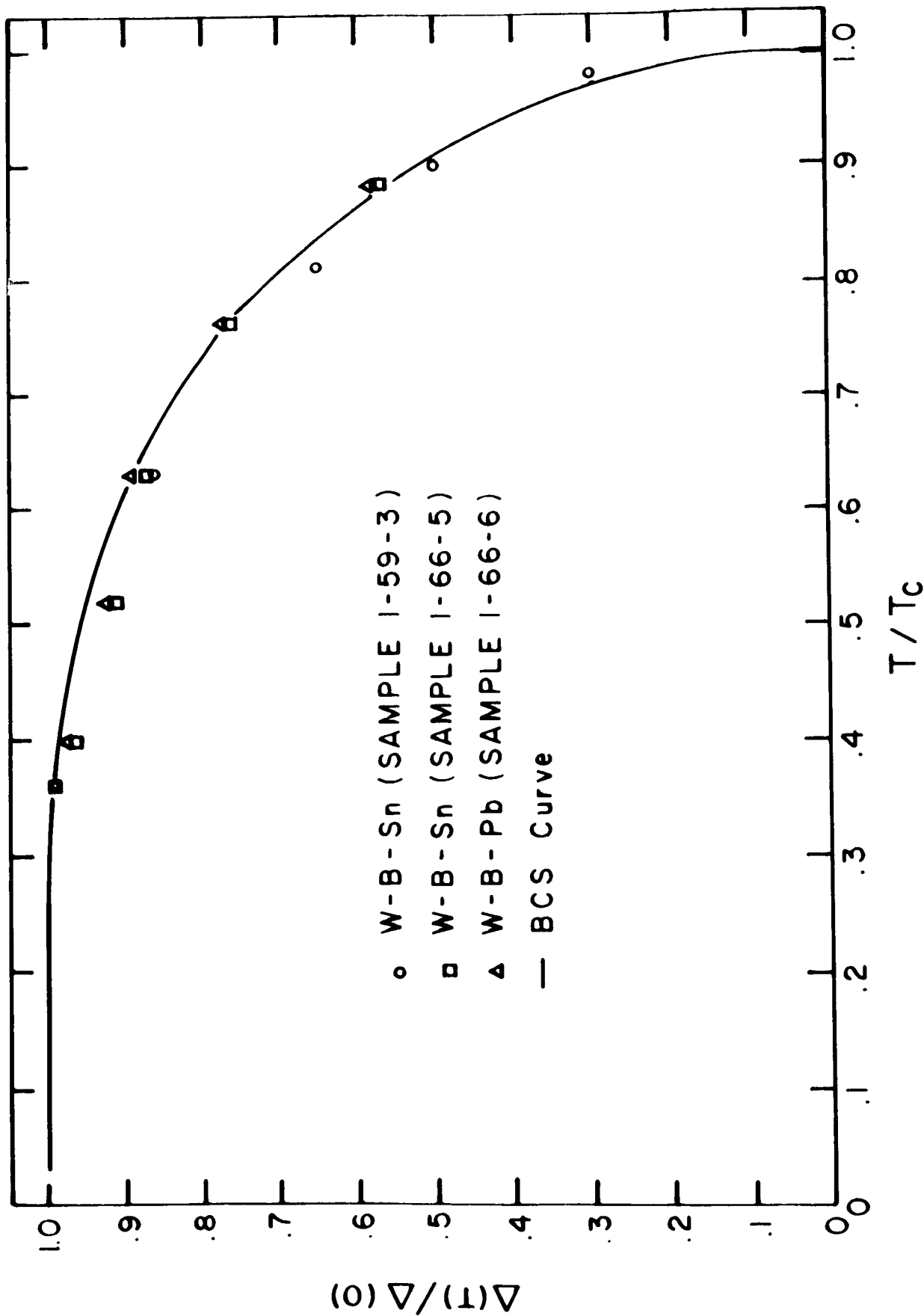


FIGURE 3.

Energy gap $\Delta(T)$ of β -W as a function of temperature T . T_c varied from 3.1°K to 3.3°K and the corresponding value of $2\Delta(0)/kT_c$ are 2.63 and 3.64 respectively.

Studies of Thermal Transpiration for the
Development of a "Thermal Pump"

Senior Investigator: Dr. Manfred Altman

Graduate Student: E. Hopfinger

Thermal transpiration, the phenomenon of the flow of gases through porous media under the influence of a temperature gradient, can be utilized as a driving force in a new type of gas pump. In previous reports the phenomenon of thermal transpiration was described and the following was reported:

- 1) Flow rates through an ideal barrier, i.e. infinitely thin and a pore size much smaller than the molecular mean free path, calculated from kinetic theory.
- 2) Experimental results of flow rates and steady state pressure differences as a function of mean pressure, typical of thermal transpiration in membranes of finite thickness.
- 3) A theoretical formulation of thermal transpiration in actual membranes, based on the methods of non-equilibrium thermodynamics and the dusty-gas theory¹. The equations evolved predicted the experimental results adequately.

In this report thermal transpiration for the use of power production is analyzed more closely. A generalized treatment of linear systems was developed by Odum and Pinkerton².

The reduced efficiency (overall efficiency divided by Carnot efficiency) is given by

$$\eta' = \frac{\text{Power output}}{\text{Power input}} \quad (1)$$

Expressions for the power input and output in terms of the fluxes and thermodynamic potentials are obtained from the equation for the rate of entropy production. Temperature times the rate of entropy production is the rate of dissipation of energy, which is equal to the useful power input minus

the useful power output. Starting with the expression for the entropy production, Ref. (2) found an expression for the reduced efficiency in the form,

$$\eta' = \frac{r}{1 + l/[cf^2(1-r)]} \quad (2)$$

where l , c and f are general coefficients and r is a "throttle setting".

The group (cf^2/l) represents a "merit factor". Maximum efficiency and efficiency at maximum power in general occur at different values of r . When $M' \ll 1$ however, peak efficiency and peak power coincide at $r = 1/2$ and the reduced efficiency is then given by

$$\eta_{\max} = \frac{M'}{4} \quad (3)$$

For the purpose of expressing the merit factor in terms of physically more meaningful quantities, a "thermal transpiration flow coefficient" K_T was introduced in this work, similar in its nature to the isothermal permeability coefficient K . We defined K_T as $(R\bar{T}/\bar{p})$ times the molar rate of flow per unit area of membrane, at zero pressure difference, divided by the temperature gradient*. In terms of K_T the merit factor can be expressed as

$$M' = \bar{T} \bar{p} \left(\frac{K_T^2}{K \kappa} \right) \quad (4)$$

* In previous reports a different definition for K_T was given.

where \bar{T} and \bar{p} are the mean temperature of the membrane and mean pressure respectively, K is the isothermal permeability and κ the apparent heat conductivity and is experimentally obtained from

$$\kappa = \left[(J_1)_{J_2=0} \right] L / \Delta T \quad (5)$$

where $(J_1)_{J_2=0}$ is the energy flux at steady state, L the thickness of the membrane and ΔT the temperature difference.

Experimental results:

Experiments were carried out on five porous ceramic and two Millipore filter of different geometric properties. The geometric properties of these membranes are listed in Table 1. Fig. 1 shows a typical plot of efficiency η versus total flow rate for He at $\bar{T} = 403^{\circ}\text{K}$, $\Delta T = 106^{\circ}\text{C}$ and atmospheric pressure. The merit factors and maximum reduced efficiencies for He in all the membranes, at atmospheric pressure and those pressures at which $M'\kappa$ has a maximum value, are listed in Table 2. Also shown in Table 2 are measured values of κ . The value at which $M'\kappa$ is a maximum is seen from Table 2 to be about 1.75. A theoretical value of d_e / λ for maximum power output was derived and was found to be $(d_e / \lambda)_{\text{theor.}} = 2.13$. Table 2 shows that the reduced efficiencies for pumping helium vary from 0.001% in ceramic 06 to 0.30% in Millipore membrane GS. The variation of the efficiencies with the ceramics is due to the difference in their geometric properties as seen from Table 1. The efficiencies measured with the Millipore membranes are higher than those measured with the ceramics. This is due to the lower heat conductivities of the Millipore membrane.

The efficiency of 0.30% in the case of the Millipore GS membrane was measured at a mean pressure of 32 cm Hg. Since the efficiency, as seen from equation (4), is directly proportional to the pressure at which the pump is operated, we can conclude that an efficiency of the order of 1% can be achieved with a membrane whose physical properties are similar to those of Millipore GS, except with a pore size such that $d_e / \lambda \approx 2$.

The experiments have been completed and presently the results are compiled for the final presentation in a doctoral dissertation.

REFERENCES

- 1) E. A. Mason, R. B. Evans III and G. M. Watson, Journal of Chemical Physics 38, 1808 (1963)
- 2) H. T. Odum, and R. T. Pinkerton, American Scientist, 43, 331 (1955).

TABLE 1. GEOMETRIC PROPERTIES OF THE POROUS MATERIALS

Material	Thick- ness L cm.	Porosity ϵ	B_0 10 ¹¹ cm.	Pore diam. de 10 ⁴ cm.	$P_{crit.}$ Lb.	Pore diam. de 10 ⁴ cm.	Tortuosity τ	$D_k \sqrt{M}$ calc. cm ² sec ⁻¹	$D_k \sqrt{M}$ cm ² sec ⁻¹
Selas 06	.520	.29	.85	.48	46	.902	2.64	.250	.233
Selas 04	.627	.36	3.63	.89	32	1.30	2.06	.748	.716
Selas 03	.608	.55	15.90	1.52	26	1.62	1.50	2.64	2.54
Selas 02	.599	.54	41.40	2.46	15	2.80	1.62	3.86	4.01
Selas 01	.597	.73	961	10.3	2.5	16.8	2.32	15.0	14.2
Millipore Gs	.0145	* .74 (.75)	6.24	.823 (.22)	48	.864	1.50	1.93	1.44
Millipore VF	.0135	* .44 (.70)	.111	.142 (.010)	—	—	—	.214	.192

+ Calculated from slope of permeability curve using $k_o q^2 = 5.0$

++ From critical capillary pressure experiments

* Determined from wet and dry weights; the numbers in parentheses are the values specified by the manufacturer

TABLE 2. Experimental values of the merit factor, reduced efficiency and efficiency with Helium in all the ceramics and the millipore membranes.

SYSTEM	\bar{P} cm Hg	\bar{T} °K	d_e/λ	$10^5 K_T$ $\text{cm}^2 \text{sec}^{-1} \text{°C}^{-1}$	K $\text{cm}^2 \text{sec}^{-1}$	$M'K$ ergs per cm sec °C	κ cal per cm sec °C	$10^3 \eta'_{\max}$ %	$10^3 (\eta_{\max})_{\Delta T=100^\circ \text{C}}$ %
He in ceramic 06	76 34	361 361	3.77 1.69	6.5 9.7	.1654 .1447	9.45 10.83	.00522 .00497	1.073 1.282	.297 .355
He in ceramic 04	76 26	385 385	5.1 1.74	16.2 29.5	.559 .457	18.6 25.8	.00408 .00390	2.68 3.89	.695 1.01
He in ceramic 03	76 20	371 371	6.58 1.73	52.5 107.0	2.14 1.61	49.2 72.5	.00245 .00219	10.75 19.40	3.17 5.23
He in ceramic 02	76 13	375 375	11.28 1.93	49.5 157.0	4.09 2.54	23.1 41.3	.00256 .00223	5.28 10.92	1.41 2.91
He in ceramic 01	76 2.8	371 371	68.3 2.5	37.7 518	62.48 9.88	0.78 38.3	.00219 .00166	.234 13.55	.063 3.65
He in millipore Gs	76 32	334 334	3.91 1.64	38 65	1.092 .919	45.6 66.7	.000158 .000129	170.0 303.0	50.8 90.7
He in millipore VF	76	320	.680	9.7	.1036	29.9	.000184	95.5	29.8

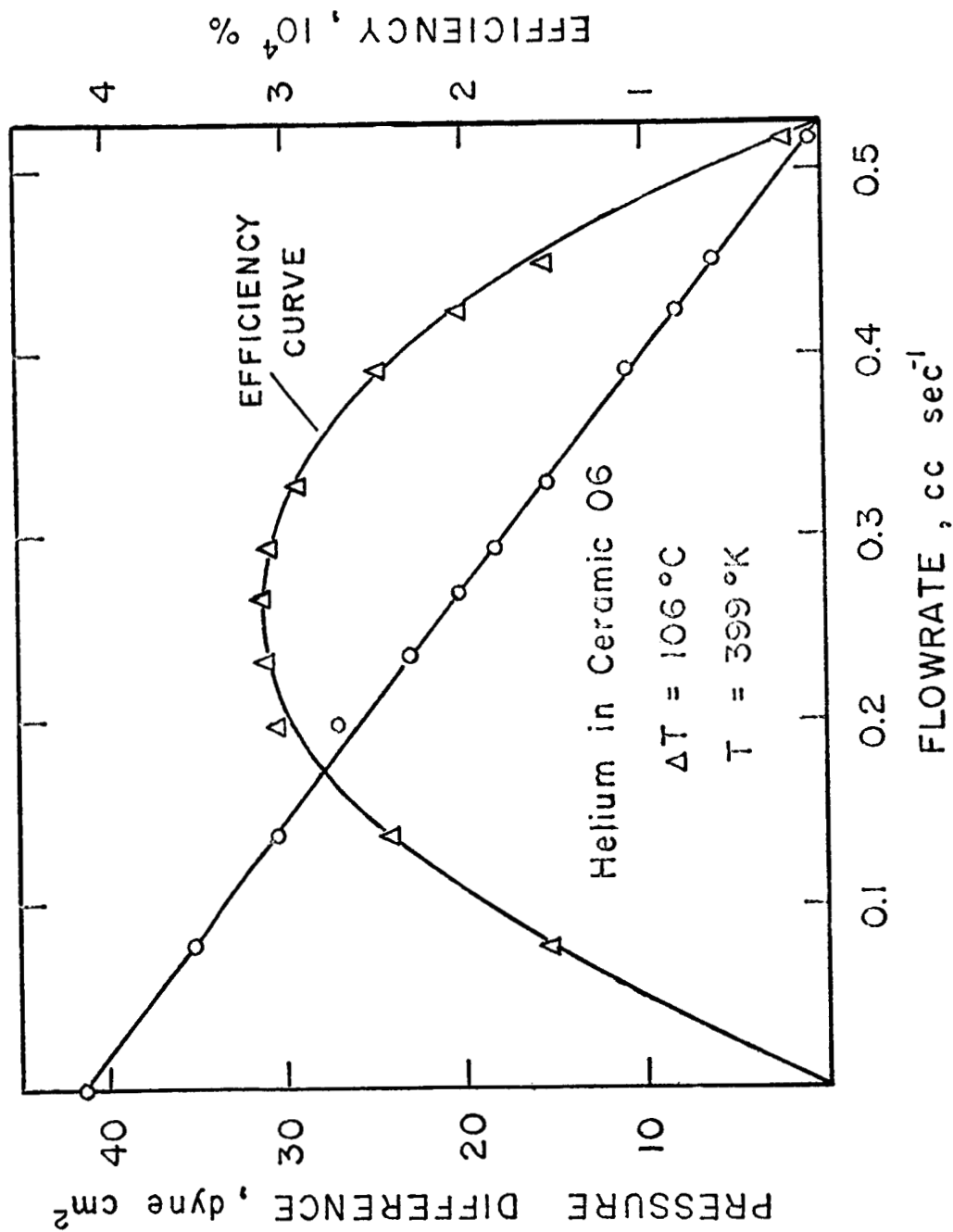


Fig. 1. Pressure-difference and efficiency vs. flow rate for helium in ceramic O6, at atmospheric pressure.

Preparation and Structure of Barium-Graphite Alloy

Barium and pyrolytic graphite have been combined as a result of vacuum diffusion anneals in stainless steel crucibles according to the schedule of heat treatments shown in Table 1.

Table 1: Times and Temperatures for Diffusion Anneals

<u>Temperature ($^{\circ}\text{C}$)</u>	<u>Time (hrs.)</u>
925	50, 150, 300
750	200, 400, 600
635	100, 200, 300, 400
575	400, 500

A shiny golden barium-graphite compound has formed as a result of diffusion anneals for all temperatures reported. Although the compound is unstable in air at room temperature, it is stable in vacuum or inert atmosphere. The most immediate change noted is a dimensional one. The height in the "c"-direction doubles with no apparent variation in the "a"-direction dimensions. In all cases the mechanical integrity of the resulting sample is maintained as no exfoliation is noted. Covering its external surface is a thin dark gray crust of barium carbide.

When specimens are cleaved perpendicular to the "c"-axis, samples heated at 575°C and 635°C show the gold compound surrounding a black core with a clearly defined interface. The interface proceeds toward the specimen's center with longer annealing times. In graphite compounds, the golden material is indicative of the maximum interstitial concentration. One could, therefore, expect C_8Ba to exist in the entire golden region having a constant concentration of barium at the moving interface. With

barium atoms placed between the layers, the tendency is to lift the layers. One would therefore expect that some barium would diffuse into the core. The appearance of minute golden pieces in the core indicates that some barium has found a path of easy diffusion and has attained the maximum concentration.

At higher temperatures of annealing, the interface for compound formation was not observed. There is a distant lack of homogeneity as blue and gold portions are seen to be interspersed with graphite and barium carbide. The bluish tinted material is believed to be a graphite compound with lower than maximum concentration.

The graphite compound formed (pending chemical analysis) is believed to be C_8Ba . X-Ray data has shown the distance between (001) planes to be 5.28 \AA . The distance between carbon layers in the compound represents a sizeable increase over the parent graphite which was measured to be 3.34 \AA . It is also observed that there has been a shift in lattice parameter in the "a"-direction from 2.46 \AA for graphite to 2.49 \AA for compound. This would indicate that the addition of barium as an interstitial strains the basal layers of carbon atoms.

Electron microscopy has been performed on heat treated specimens. Measured values of (100) and (110) reflections are seen in Table 2.

Table 2: Comparison of Lattice Distances between
(100) and (110) Planes

<u>Reflection</u>	<u>Graphite</u>	<u>Core Material</u>	<u>Compound</u>
(100)	2.12	2.13	2.15
(110)	1.22	1.23	1.24

A good agreement in these basal plane distances is noted. The small deviation for compound can not be definitely attributed to barium addition since the deviation is well within the limit of error of microscopy measurements. Expanded parameters in the "c"-direction were not substantiated by electron microscopy. This lack is attributed to the inability to transfer the compound material to the microscope without reaction with air. Another possibility is that the electron beam may be destroying the compound and tending to form a residue compound which approximates the parent graphite structure.

The question of stability is of key importance when concerned with graphite compounds. Upon exposure to air of the present compounds, changes in appearance are quickly noted. A whitish layer forms along the sides of the specimen parallel to the "c"-axis. Thin gray barium carbide layers form barium carbonate and tend to separate the block along their planes. Exposed compound retains its gold color for about ten minutes. It undergoes gradual dulling till a black surface results. It is of interest to note that even after days of exposure, removal of outer layers will once again reveal shiny gold compound indicating that total change is retarded by surface transformation. To more quantitatively ascertain the stability of the compound, resistivity measurements in vacuum will be made at elevated temperatures to determine conditions for decomposition. Chemical analysis will follow to determine the reaction product.

An attempt will be made to determine the diffusivity and activation energy for barium diffusion into carbon, based on measurement of the relative depth of penetration of the compound-core interface with time.

Thermoelectric power measurements made at room temperature in air with the apparatus of J. Curry have shown a small increase in thermoelectric power from $1\mu\text{V}$ for control graphite to approximately $10\mu\text{V}$ for material exposed to air for about fifteen minutes. With longer exposure, the thermoelectric power increases to a relatively stable value of about $20\mu\text{V}$. This increase is believed to be indicative of the formation of barium carbonate and decomposition of compound material. As yet, values of thermoelectric power can not be directly attributable to C_8Ba . To determine accurate thermoelectric power values indicative of barium-graphite, measurements will be made in vacuum and at elevated temperatures.

Extended Kronig-Penney Model for Electronic Properties
of Layer Structures

This work dealt with the electronic properties of an idealized anisotropic crystal. The form of the idealized crystal consisted of sheets of matter separated by regions of void where the potential of the sheets was $-W$ and the potential of the void was by definition zero (as seen in Figures 1 & 2).

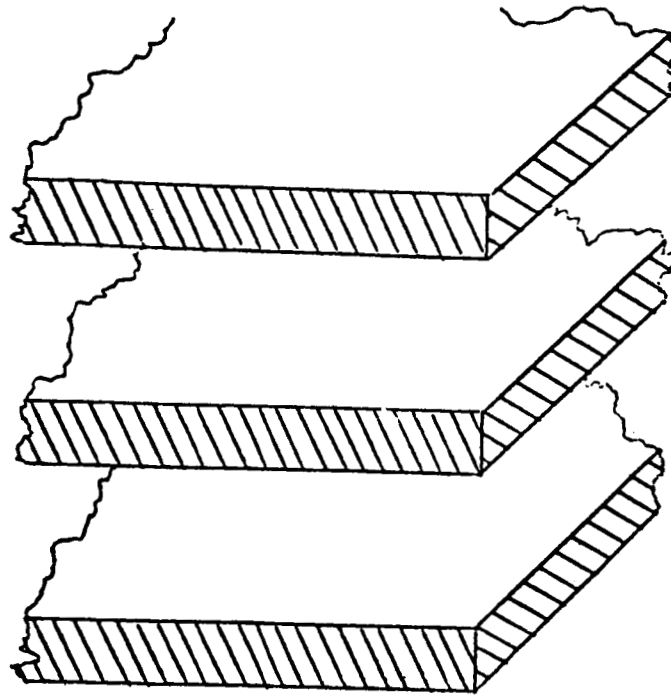


Figure 1

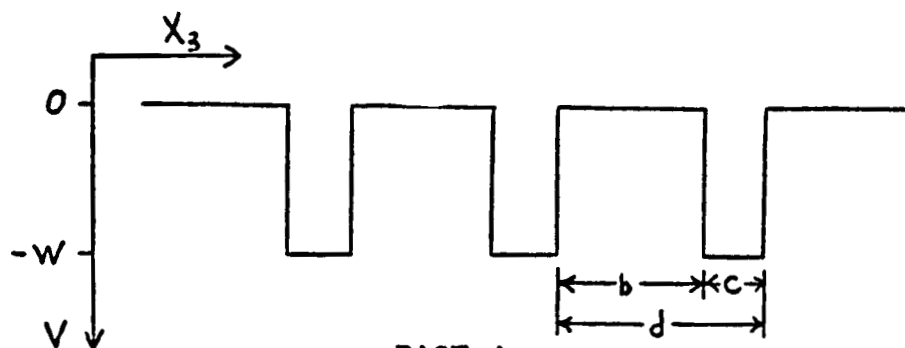


Figure 2

The reasons for looking at this particular form for the idealized anisotropic crystal were: first, in most cases of importance the number of independent components to the conductivity tensor for anisotropic crystals is two, and, by definition, this idealized anisotropic crystal has two conductivities, the conductivity in the plane and the conductivity perpendicular to the plane; second, the form of the potential was particularly amenable to calculations. Using this potential, it was a comparatively easy matter to calculate the band gaps, band widths, effective masses, and dispersion relations in the k_z direction. With $E_z(k_z)$ it was possible to construct energy contours. As a result of these contours it was seen that, depending on the parameters and the number of electrons per unit cell chosen, the model may range from an almost free electron metal to a substance with completely free electron properties in the planar direction and completely insulating properties in the perpendicular to the plane direction. This, in fact, is the prime asset of the model; that is its flexibility which arises from the parameters. It was found that a proper choice of parameters reproduced some of the qualitative features of the Fermi surface of graphite. It is expected that if the proper parameters were picked then the model would give a good qualitative description of the electronic properties of a crystal structure requiring only two independent components to the conductivity tensor (i.e. a tetragonal, a trigonal, or an hexagonal structure). Finally, the model was extended to include an impurity sheet between every two normal sheets, but the number of parameters generated by such a model made the extension unfeasible.

Lattice Thermal Conductivity of Graphite Compounds

The lattice dynamics of the lamellar compounds of graphite is that of the graphite lattice with sheetlike defects. The parameters characterizing the dynamical behaviour of the defects are evaluated in the acoustic limit. The effect of the defects on phonon transport is then given in terms of a relaxation time. The phonon relaxation times resulting from the anharmonic interactions are determined in an empirical way from the conductivity data in the literature. The frequency and temperature dependence of these relaxation times changes with the temperature of operation and so they are determined separately for low temperature and for temperature $>300^\circ\text{K}$. A combination of the defect relaxation time with those of the anharmonic interactions enables one to calculate the thermal conductivity of the compounds as a function of temperature and the concentration of the solute in the compound.

The ratio of the phonon thermal conductance κ_c in the c-direction of the compound to that of ideal graphite- κ at 300°K is about $\frac{1}{3}$ for a compound with the formula C_{48}M ; at 1000°K it is about $\frac{2}{3}$. The peak of the conductivity κ_c occurs at 60°K while that of κ at 30°K the ratio of the peaks being $\sim\frac{1}{5}$. The variation with concentration is more significant at low temperatures.

At higher metal concentrations the ratio of phonon conductivity of compound to that of graphite will be smaller. However, the contribution of conduction electrons to thermal conductivity increases with increasing metal concentration. Computations in this high concentration range are in progress.

ELECTROCHEMICAL ENGINEERING

APPENDIX

A-3

Overpotential Transients on the Rotating Disk

Senior Investigator: Dr. L. Nanis

Graduate Student: Irving Klein

A rotating disc anode is to be operated under galvanostatic conditions until a steady state value of the overpotential is attained. The current is then to be interrupted and a recorder will plot the resulting transient overpotential. A mathematical model has been proposed to enable one to predict this transient. The model requires a solution to a one dimensional, time-dependent Navier-Stokes relation, equation (1), subject to the boundary conditions specified in equation (1A) and equation (1B) and the initial condition set in equation (1C).

Note that equation (1C) is a power series expression corresponding to the solution given by Levich^(R-1) for the steady state concentration profile on rotating disc electrodes.

$$\frac{\partial \psi}{\partial \tau} = P_e(\xi) \frac{\partial \psi}{\partial \xi} + \frac{\partial^2 \psi}{\partial \xi^2} \quad \text{Eq. (1)}$$

$$\frac{\partial \psi(0, \tau)}{\partial \xi} = 0 \quad \text{Eq. (1A)}$$

$$\psi(1, \tau) = 0 \quad \text{Eq. (1B)}$$

$$\psi(\xi, 0) = 1 - 1.572 \left[\xi - \frac{\xi^4}{1.457} + \frac{\xi^7}{1.859} - \frac{\xi^{10}}{2.905} + \frac{\xi^{13}}{5.503} - \frac{\xi^{16}}{12.34} + \frac{\xi^{19}}{30.37} - \frac{\xi^{22}}{94.7} \right] \quad \text{Eq. (1C)}$$

ψ - dimensionless concentration - $\frac{c - c_b}{c_o - c_b}$

τ - dimensionless time - Dt/δ^2

ξ - dimensionless distance - y/δ

P_e - peclet no. - $V_y \delta / D$

D - diffusion coefficient - cm^2/sec

y - distance perpendicular to the surface of the disc - cm

t - time - sec

R-1 Levich, V.G. Physicochemical Hydrodynamics, Prentice Hall, N.J.
1962

- δ - diffusion boundary layer thickness, corresponding to the point along the y coordinate at which ψ attains 99% of its bulk value - cm
- c_o - concentration of the anodic species at the surface of the disc at zero time - g/cm³
- c_b - concentration of the anodic species in the bulk - g/cm³

A solution to the preceding partial differential equation was obtained by two different techniques: (a) It was assumed that Pe' is constant throughout the boundary layer and analytical solutions of this approximation to the differential equation were obtained for various values of Pe' . (b) The partial differential equation was numerically solved on a computer by relaxation techniques.

The next step will be an experimental certification of the mathematically derived ψ vs τ results.

Note, however, that it is critical for the surface of the rotating disc anode to remain perfectly smooth throughout the duration of the experimental run. It was recognized that a redox reaction would ideally suit this purpose, and an expression was derived, equation (2), that mathematically predicts the behavior of the total transient overpotential on a rotating disc anode.

$$\eta = \frac{zF}{RT} \ln \left\{ \frac{\psi^A (-\alpha \gamma) + 1}{\psi^B (\beta \gamma) + 1} \right\} \quad \text{Eq. (2)}$$

η - overpotential - volts

T - temperature - °K

R - gas constant - calories/ g mole °K

z - g equiv./ g mole

F - Faraday constant

$$\gamma = \left(1 - e^{zF\eta_o^T/RT} \right) / \left(e^{zF\eta_o^T/RT} \cdot \frac{c_b^B}{c_b^A} + \left(\frac{D^B}{D^A} \right)^{\frac{2}{3}} \right)$$

$$\beta = c_b^A / c_b^B$$

$$\alpha = (D^B/D^A)^{\frac{2}{3}}$$

- A - used as a superscript refers to oxidized anodic species
- B - used as a superscript refers to reduced cathodic species
- o - used as a subscript refers to conditions at time zero
- b - used as a subscript refers to conditions in the bulk

$$\psi^A - \text{dimensionless concentration} - \frac{c_{y=0}^A - c_b^A}{c_{y=0}^A - c_b^A}$$

$$\psi^B - \text{dimensionless concentration} - \frac{c_o^B - c_b^B}{c_o^B - c_b^B}$$

ψ^A and ψ^B are mathematically obtained by using the solutions of equation (1).

Attention is presently directed to equipment construction, choice of a suitable redox system and the preparation of curves of expected transients.

Current and Potential Distribution in Cylindrical Geometries:
Engineering Application to Fuel Cell Design

Senior Investigator: Dr. L. Nanis
Graduate Student: Wallace Kesselman

It was shown in the last quarter that treatment of the two-dimensional Laplace equation in cylindrical coordinator with no angular dependence, by means of the Fourier-Bessel (Hankel) transform, and application of the boundary condition describing a linear overpotential relationship on the disc in an insulating plane, viz.

$$J(r) = -\kappa \frac{\partial V}{\partial z}(r) = J_0 \frac{zF}{RT} \eta(r) \quad (1)$$

$$J(r) = 0 \quad (2)$$

$$\text{where } V_0 = \text{constant} = V(r) + \eta(r) \quad (3)$$

will yield the following description of the phenomena occurring at the plane

$$V(r) = \int_0^\infty A(p) J_0(pr) dp \quad (4)$$

$$\frac{\partial V}{\partial z}(r) = -\int_0^\infty p A(p) J_0(pr) dp \quad \text{and} \quad (5)$$

$$V_0 = \int_0^\infty A(p) J_0(pr) dp + c \int_0^\infty p A(p) J_0(pr) dp \quad (6)$$

$$0 = \int_0^\infty p A(p) J_0(pr) dp \quad (7)$$

$$\text{where} \quad c = \frac{\kappa RT}{J_0 z F} \quad (8)$$

The problem of convergence reported in the last quarter can be avoided by proceeding on a slightly different track from this point on. First, we rewrite equations (6) and (7) as follows:

$$\int_0^{\infty} \xi A(\xi) \mathcal{J}_0(\xi r) d\xi = \frac{V_0}{c} - \frac{1}{c} \int_0^{\infty} A(\xi) \mathcal{J}_0(\xi r) d\xi \quad (9)$$

$$\int_0^{\infty} \xi A(\xi) \mathcal{J}_0(\xi r) d\xi = 0 \quad (10)$$

(9) and (10) now describe the Hankel transform of $A(\xi)$. Applying the inversion formula, viz.

$$A(p) = \int_0^{\infty} r f(r) \mathcal{J}_0(pr) dr \quad (11)$$

we get

$$A(p) = \frac{a V_0}{c} \frac{\mathcal{J}_1(pa)}{p} - \frac{1}{c} \int_0^a \int_0^{\infty} x A(\xi) \mathcal{J}_0(\xi x) \mathcal{J}_0(px) dp dx \quad (12)$$

Finally, multiplying (12) through by $\mathcal{J}_0(pr)$ and integrating from 0 to ∞ , we get from Eqn. (4)

$$\begin{aligned} V(r) = & \frac{a V_0}{c} \int_0^{\infty} \frac{\mathcal{J}_1(pa) \mathcal{J}_0(pr)}{p} dp \\ & - \frac{1}{c} \int_0^{\infty} \int_0^a V(x) x \mathcal{J}_0(px) \mathcal{J}_0(pr) dx dp \end{aligned} \quad (13)$$

These integrals are of the Weber-Schafheitl type, and so we get for the potential variation

$$V(r) = \frac{2}{\pi} \frac{a}{c} V_0 E\left(\frac{r}{a}\right) - \frac{2}{\pi c} \int_0^r V(x) \frac{x}{V} K\left(\frac{x}{r}\right) dx \\ - \frac{2}{\pi c} \int_r^a V(x) K\left(\frac{r}{x}\right) dx \quad r < a \quad (14)$$

$$V(r) = \frac{2}{\pi} \frac{a}{c} V_0 \frac{r}{a} \left\{ E\left(\frac{a}{r}\right) - \left[1 - \left(\frac{a}{r}\right)^2\right] K\left(\frac{a}{r}\right) \right\} \\ - \frac{2}{\pi c} \int_0^a V(x) \frac{x}{r} K\left(\frac{x}{r}\right) dx \quad r > a \quad (15)$$

Here, K and E are the complete elliptic integrals of the first and second kinds respectively; i.e.

$$K(k) = \int_0^{\frac{\pi}{2}} \frac{d\phi}{\sqrt{1 - k^2 \sin^2 \phi}} \quad (16)$$

$$E(k) = \int_0^{\frac{\pi}{2}} \sqrt{1 - k^2 \sin^2 \phi} \, d\phi \quad (17)$$

Furthermore, through use of (1), (3), (14) and (15) and by using the following groups

$$J^* = \frac{KV_0}{a} \quad \hat{J} = \frac{J(r)}{J^*} \quad \lambda = \frac{2a}{\pi c} \quad \gamma = \frac{r}{a} \quad (18)$$

we get for the current distribution on the disc

$$\begin{aligned}\hat{J}(y) &= \frac{\lambda \pi}{2} - \lambda \int_0^y \hat{J}(\xi) \frac{\xi}{y} K\left(\frac{\xi}{y}\right) d\xi \\ &\quad - \lambda \int_y^1 \hat{J}(\xi) K\left(\frac{\xi}{y}\right) d\xi \quad r < a \quad (19)\end{aligned}$$

Hence, we now have reduced the problem of current and potential distribution to the solution of singular linear integral equations. Solution is rather straightforward using the method of Carl Wagner⁽¹⁾.

From (18) and (19), it is apparent that two parameters determine the current distribution: λ , which corresponds to the reciprocal of the group $\frac{\kappa}{a} \frac{\partial \eta}{\partial J}$, and J^* , a group with dimensions of current which contains in it the potential difference applied to the disc.

For $\lambda \ll 1$ (i.e., $\left| \frac{\kappa}{a} \frac{\partial \eta}{\partial J} \right| \gg 1$), equation (19) shows the expected uniform current density, and equation (14) and (15) reduce to the expression for potential variation previously derived for uniform current distribution. Equation (19) has been solved for various values of λ , and the results compare very favorably with those of Newman⁽²⁾. For small values of λ , current and potential distribution may be approximately represented by

$$J\left(\frac{r}{a}\right) = \frac{\frac{\pi}{2} \lambda J^*}{1 + \lambda E(r/a)} \quad (20)$$

$$V\left(\frac{r}{a}\right) = \frac{\lambda V_0 E(r/a)}{1 + \lambda E(r/a)} \quad (21)$$

Work is in progress on non-linear integral equations (also singular) describing current and potential distribution for the more general case of

the non-linear current-overpotential relationship.

REFERENCES

- (1) C. Wagner, "On the Solution of Fredholm Integral Equation of the Second Kind by Iteration," J. Math. Phys. 30, 23 (1951).
- (2) John Newman, "Current Distribution on a Rotating Disc Below the Limiting Current," J. Electrochem. Soc. 113, 12, 1235 (1966).

Foaming Electrolyte Fuel Cell

Senior Investigator: Dr. L. Nanis

Research Specialist: A. P. Saunders

In the reporting period, attention was given to determining virtual fuel cell (H_2 , O_2) operating characteristics. In order to evaluate possible impurity contributions to the cyclic behavior reported previously (INDEC-SR-12), an all Teflon cell was constructed. Cleaning was accomplished by boiling all components in concentrated nitric acid followed by washing in conductivity water. Care was taken to insure that only Teflon and platinum contacted the electrolyte which was 2 N KOH prepared from conductivity water. Even with purification, the overpotential instability persisted. Hydrogen purification was provided by a commercial silver-palladium permeation unit (Serfass CH-A hydrogen purifier). Successful dynamic purification was accomplished by passing helium rather than oxygen through the cathode compartment and by continuous helium purging of the rest of the cell except for the actual anode chamber. A measure of purification is indicated by the repeatable attainment of a reversible potential of the smooth sheet platinum with respect to a reversible hydrogen electrode in the same solution. The open circuit potential difference was generally less than 1 mV and often less than 0.2 mV. Selection of 1.5 mA cm^{-2} provided an anodic overpotential trace which indicated features common to the previous cyclic variation. For example, in Fig. 1, the time variation of overpotential shows a marked inflection in slope at 0.28 V generally corresponding to the lower limit of previous cyclic behavior. The potential of inflection is associated with the potential of zero charge on platinum and thus represents a region of possible chemi-

sorption of surfactant. The gradual rise in potential underwent a sudden reversal just as the potential reached 0.77 V. In work of this contract, this potential has been noted previously, for 1 N H_2SO_4 , as a transition for wetting behavior (G. Rowell, INDEC-SR-9, Section 4.3). One attempt of the anode to enter cycling behavior is clear in Fig. 1, followed by attainment of oxygen evolution reaction potential at 1.77 V. Fig. 2 shows the behavior of the electrode following open circuit in the same foamed 2 N KOH electrolyte as for Fig. 1. The horizontal region at 0.96 V may indicate the existence of a metastable platinum-oxygen surface phase. A rapid drop to the reversible potential (0.0 V) follows decay to 0.7 V. Under the clean conditions of hydrogen saturation in the 2 N KOH electrolyte indicated by the absence of cyclic behavior, a flow of hydrogen (less than 9 cc per min.) produced the steady anodic operating potential of 1.77 V; interruption of the hydrogen flow produced a steady value of 2.2 V in less than 10 seconds. Although electrode behavior is a composite of mixed reactions, the evidence is clear for the existence of a diffusional overpotential in the foamed system. Other surfactants are presently under study.

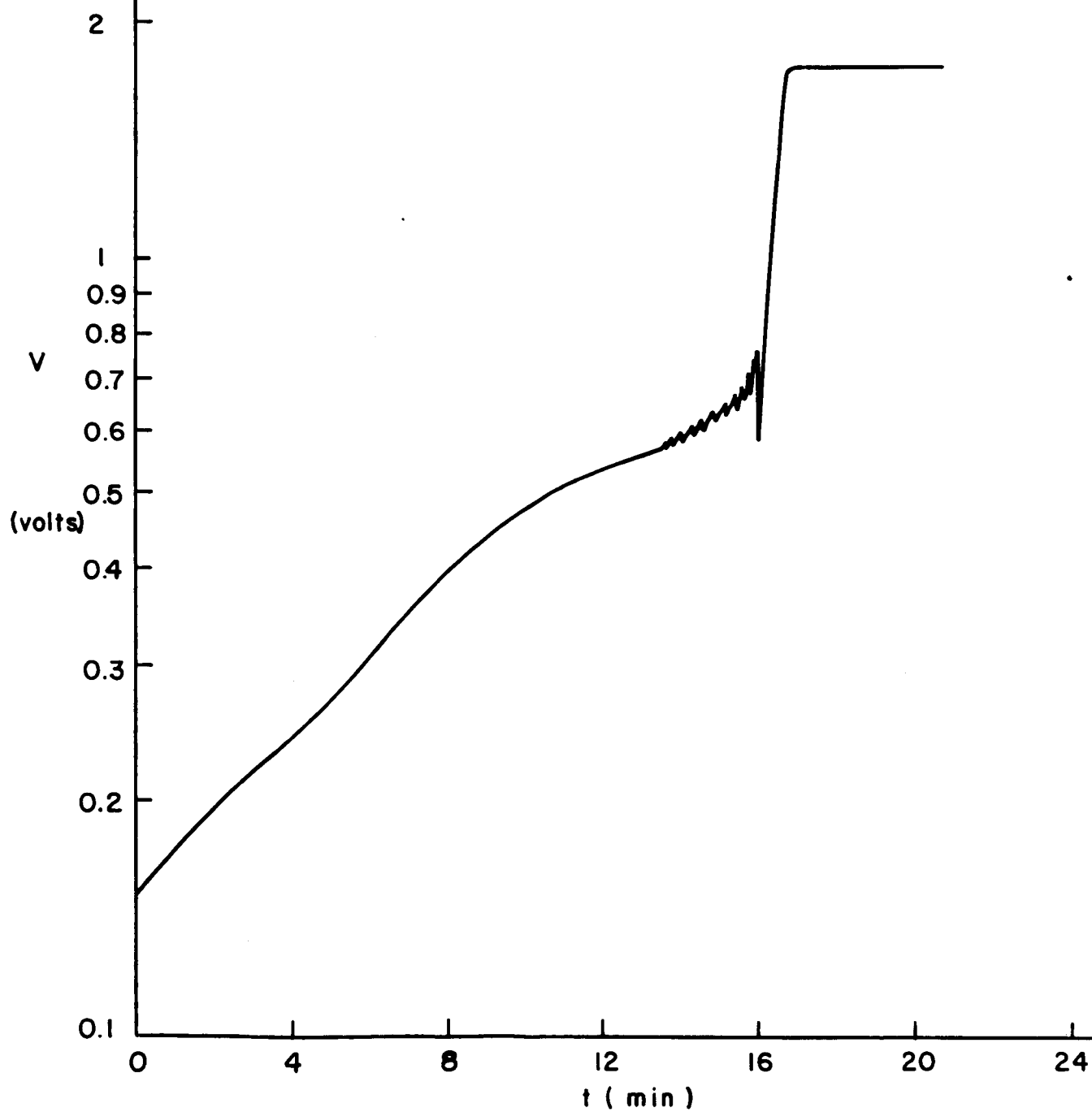
ANODE VOLTAGE vs TIME

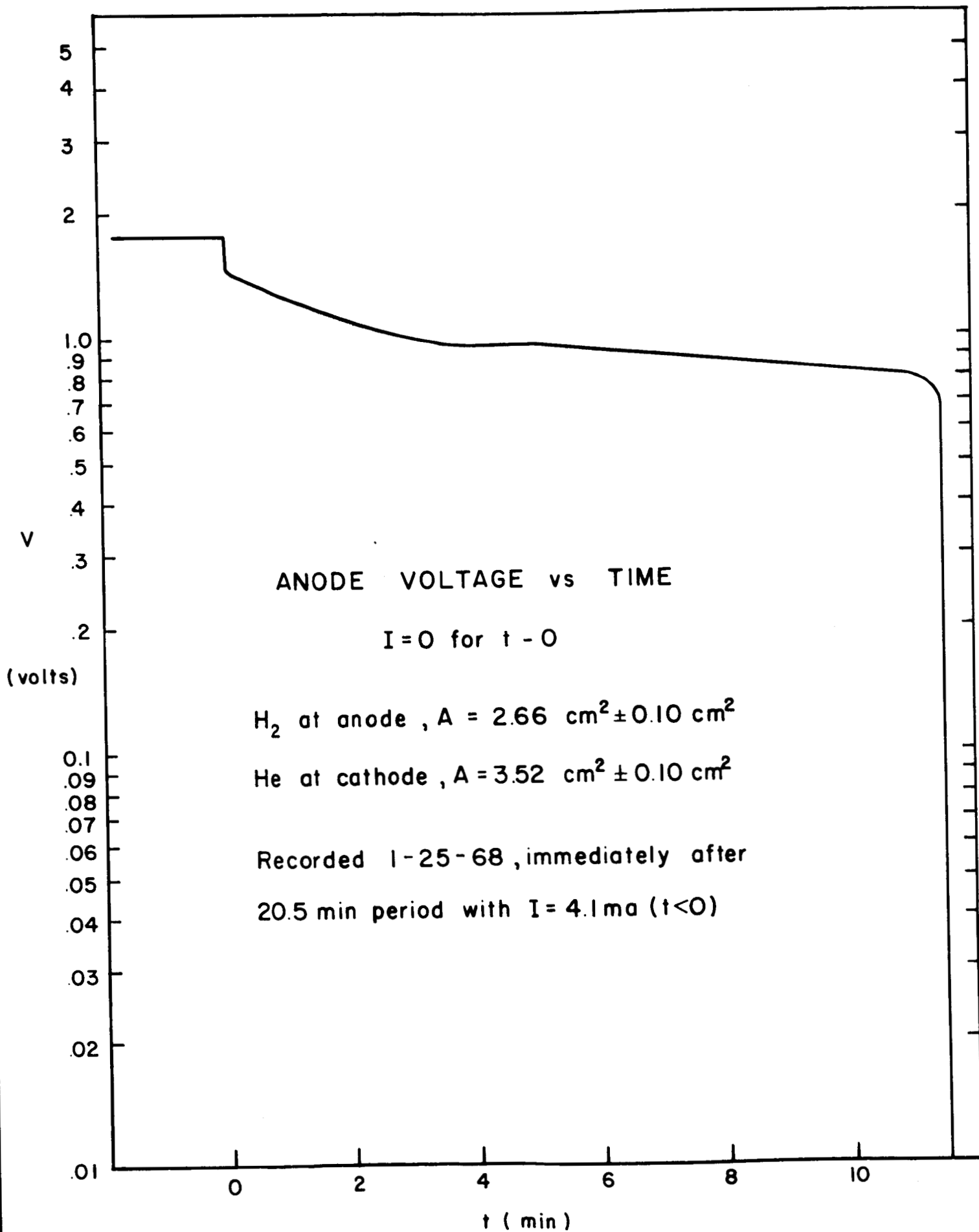
$I = 4.1 \text{ ma}$

H_2 at anode , $A = 2.66 \text{ cm}^2 \pm 0.10 \text{ cm}^2$

He at cathode , $A = 3.52 \text{ cm}^2 \pm 0.10 \text{ cm}^2$

Recorded 1-25-68





ANODE VOLTAGE vs TIME

$I = 0$ for $t > 0$

H_2 at anode, $A = 2.66 \text{ cm}^2 \pm 0.10 \text{ cm}^2$

He at cathode, $A = 3.52 \text{ cm}^2 \pm 0.10 \text{ cm}^2$

Recorded 1-25-68, immediately after
20.5 min period with $I = 4.1 \text{ ma}$ ($t < 0$)

Atomic Scale Electrode Processes:
Exchange Current Density on Iridium

P. Javet

L. Nanis

The recently developed technique of field ion microscopy (F.I.M.) is a powerful tool for the investigation of metal surfaces. In many instances, resolution of individual atoms in the metallic lattice has been possible⁽¹⁾. Recent progress in electrode kinetics has shown the need for models on a true atomic scale for the interpretation of phenomena occurring at the electrified interface.

The use of F.I.M. for electrochemistry provides an opportunity to observe surface effects on a scale in which the elementary electrochemical steps occur. Experiments have been performed based on the sequence:

- 1) image iridium tip (after shaping to almost perfect hemispherical form and atomic smoothness by field induced evaporation);
- 2) bring to atmospheric pressure and remove tip from F.I.M.;
- 3) immerse for specified time in electrolyte with iridium ions;
- 4) rinse electrolyte from tip;
- 5) return to F.I.M. and image again.

Changes on the surface have been photographically recorded and compared with those occurring in a "blank" experiment during which the tip is treated in a similar electrolyte, but free of iridium ions.

The rate of exchange of charge at the equilibrium potential between a metal and its ions is the exchange current density, a central concept of electrode kinetics⁽²⁾. Thus, rearrangement of a previously smooth surface should be expected as atoms from the metal become involved in the exchange of charge. The extent of this perturbation is expected to be an increasing function of the time of contact of the metal with the electrolyte and of the magnitude of the exchange current. F.I.M. prepared iridium tips have been immersed for various times in acid solution (2 N H₂SO₄) containing 10⁻⁶ molar iridium ion. A blank experiment using the same acid without iridium ions has shown that the surface perturbation extends only 3 ± 1 atom layers. For the solution containing iridium ions, however, the perturbation extends very much deeper than three layers. The relationship between the time of contact with solution and the depth of penetration (corrected for blank) is shown in Fig. 1. Correlation of the observed atom redistribution with time of immersion, exchange current density and, e.g. crystallographic factors is presently under study. However, two important features are readily obtained from the immersion experiments:

a) For brief times of contact (less than 5 min.), comparison of the damage which occurs in various crystallographic directions permits ordering of relative exchange current density on different crystal faces as

$$J_o(111) < J_o(100) < J_o(210)$$

A similar order

$$J_o(111) < J_o(100) < J_o(110)$$

has been determined for copper (f.c.c., as is iridium) by Damjanovic et. al.⁽³⁾ in a study of electrodeposition kinetics.

b) With prolonged contact (greater than 5 min.) between the metal and its ions, the formation of "spikes" on the surface has been observed.

Fig. 2 shows a field-evaporated clean iridium tip with a central (100) region. The four-fold symmetry decoration is caused by field-stabilized protruding atoms in the [110] directions. The nearly hemispherical tip has an average radius of curvature of about 800 Å.

Following imaging, this tip was immersed for ten minutes in iridium ion solution as mentioned above. Fig. 3 shows the image of the treated tip after the removal of 10 atom layers by field evaporation. The two "spikes" are centered around the [310] direction and appear with a higher magnification and resolution than for the corresponding regions in Fig. 2, due to the smaller radius of curvature of the "spikes".

By postulating a simple model for the transfer of material on the surface, an estimate for the magnitude of the exchange current density may be obtained. It has been observed that a general roughening of the entire surface occurs during the first five minutes of immersion, followed by a growth pattern which favors specific directions (Fig. 3). Accordingly, suppose that all discharge of ions after five minutes takes place at the favored position, causing this region to grow, i.e. a hypothetical separation of the cathodic and anodic components of the exchange current density.

The approximate volume of the spike region may be readily computed from direct measurements of the area at different levels as layers are removed by field evaporation. Using Figs. 2, 3 and images at other levels, assuming a tetravalent iridium ion, an upper limit of $10^{-4} \text{ A cm}^{-2}$ for the exchange current density is obtained.

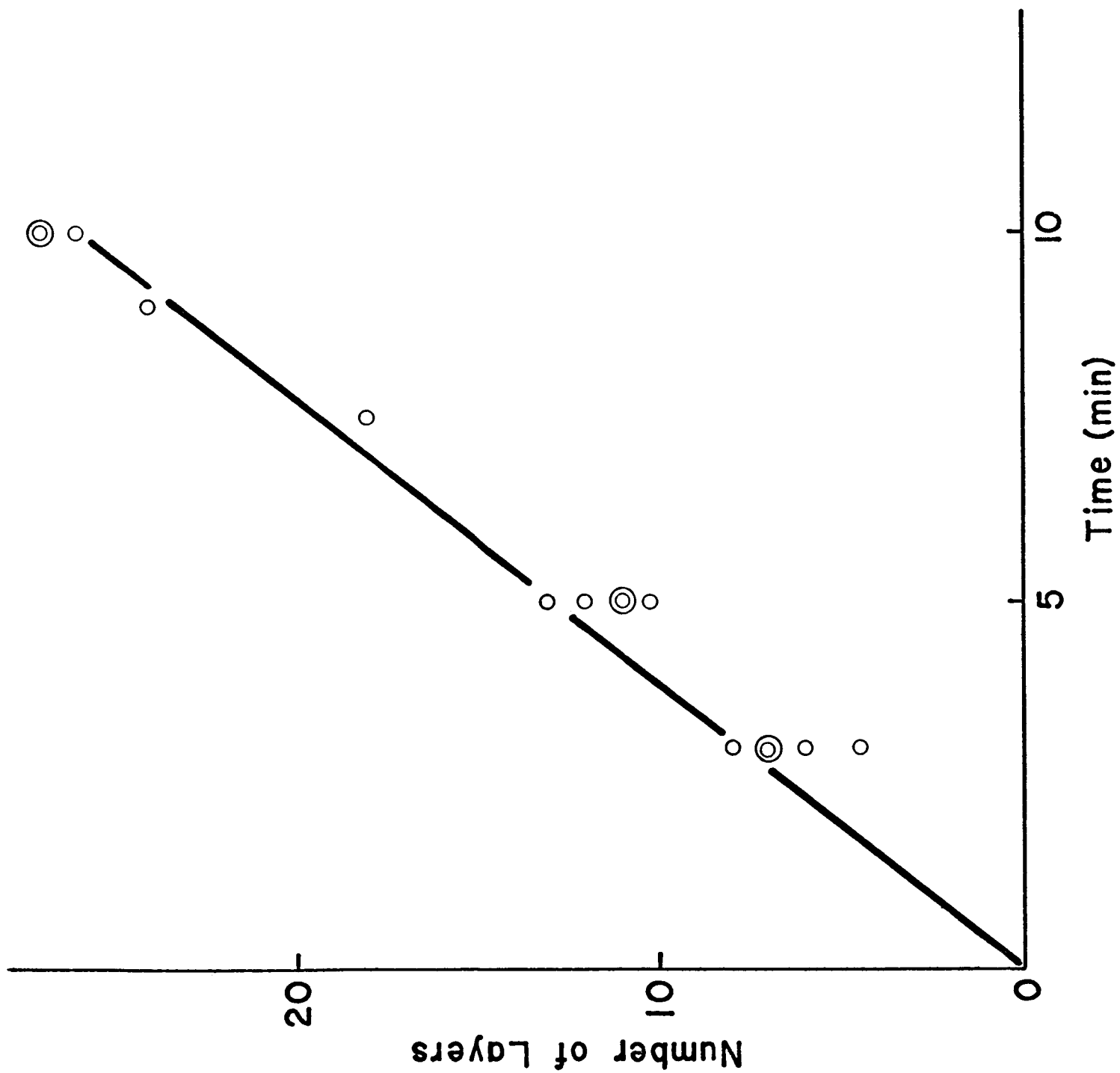
It is expected that direct F.I.M. observation of treated electrode surfaces will be helpful in devising models for electrochemical reactions, not only by the observation of the changes induced on the surface by electrochemical treatment, but also through consideration of the analogy between the field used for image formation and the field at the electrode-electrolyte interface.

Dislocations are absent from the growth features in Fig. 3, suggesting that mechanisms exist for electrocrystallization which do not require spiral dislocations to initiate and maintain growth. Some of the well-known features of the F.I.M. method such as field-stabilized protruding atoms (four-fold decoration in Fig. 2) and field-induced mechanical stresses require incorporation in models of the electrochemical interface.

This work supported by NASA Grant NSG-316.

References

- (1) E. W. Müller, "Advances in Electronics," 13, 89 (1960).
- (2) H. Gerischer, Z. Elektrochem. 54, 362 (1950); 55, 98 (1951); 59, 604 (1955).
- (3) A. Damjanovic, T. H. V. Setty, J. O'M. Bockris, J. Electrochem. Soc. 113, 429 (1966).



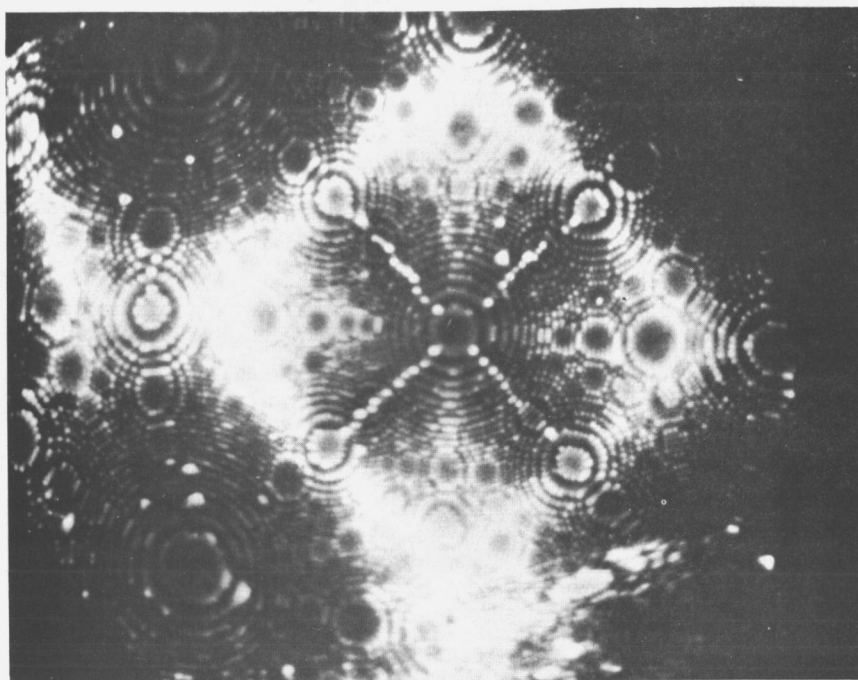


Figure 2

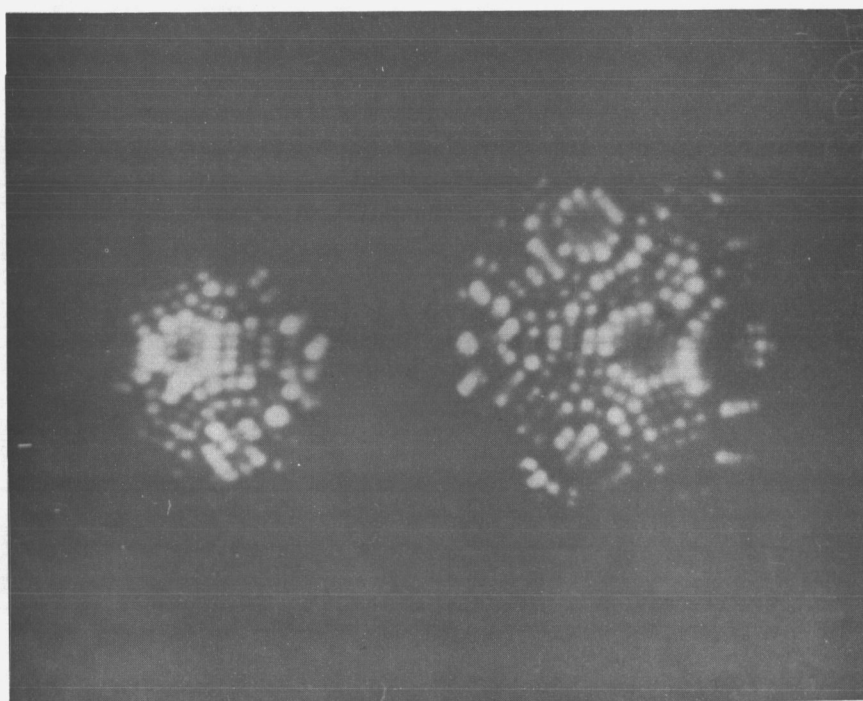


Figure 3

FIGURE CAPTIONS

- Fig. 1: Number of perturbed layers on Iridium tip as a function of time of contact with Iridium ions.
- Fig. 2: Field ion image of smooth, field evaporated Iridium tip before electrochemical treatment; (100) plane in center, (111) planes in picture corners. Image potential 17.3 kV; Imaging gas helium 2 μ m Hg.
- Fig. 3: Iridium tip, same as Fig. 2, after 10 minutes contact with solution, 10^{-6} m Ir, followed by return to F.I.M. and field evaporation of 10 atomic layers. The two "spike" growth features are each centered on [310] directions. 11.5 kV; 2 μ m Hg helium. Imaging potential 11.5 kV; Imaging gas helium, 2 μ m Hg.

PRIMARY AND SECONDARY CELLS USING CHARGE TRANSFER COMPLEXES

In previous work¹ the complex Phenothiazine/I₂, with a stoichiometry of 1: 1.5 was prepared by simply grinding the two components singly and then together with a mortar and pestle. The powdered complex was then pressed between carbon and magnesium electrodes to form a sandwich construction. Short circuit currents of microamps when operated in a dry atmosphere could be increased by two orders of magnitude when water vapor or acetonitrile vapor was introduced. Benzene, CCl₄ or other liquids with a low permittivity 'killed' the cell.

In the present study, a sandwich cell was made with freshly ground complex, in which the components had good adhesion. Compound which had been prepared several days earlier however, produced an assembly in which the magnesium easily separated from the complex, the complex being much harder and of a more vitreous nature than the freshly ground material. Obviously the reaction was not completed by the grinding technique and in order that a method could be found to accelerate the reaction to produce stable, reproduceable material, the two components after being ground together were sealed off under a helium atmosphere in a glass ampoule and heated in an oven at 95°C for three hours before being slowly cooled. Complexes with I₂/Ph ratios varying from 0.75 to 2 to 1 were made and the electrical resistivities measured. These measurements show values falling to a minimum of 4 ohm/Cm at a 1.5 : 1 ratio, but have yet to be confirmed. The 2:1 complex differed from the other materials in that it was soft and had a tar-like constituency. Other powders were prepared varying the I₂/Ph ratios from 0.75 to 2.5 to 1 and heated to 120°C for three hours. All of the compounds above a 1.5 : 1 ratio were soft, and although no viscosity measurements have been made, the viscosity apparently decreases with increasing I₂ content. This new material has not been investigated further at this time, but it is thought to be either a high temperature phase material which will slowly convert back to the harder compound with time, or a

modification of the Phenothiazine itself. (Tarlike compounds are known with phenothiazine derivatives when complexed with I_2). Should its properties, apart from the viscosity, remain unchanged, it will prove very useful in fabricating cells. The low I_2 content material was still hard and glassy. Attempts to cut the pressed powder plaques into bars suitable for D. C. resistivity measurements were unsuccessful. To avoid having a special press tool and die made to produce these bars, a novel technique was devised. A steel disc, exactly the inner diameter of the press die (1") and 8 m/m thick was cut to remove a bar 5 m/m wide from its center, leaving two symmetrically shaped pieces which were placed in the bottom of the press die. The complex powder was then compacted into the formed slot by hand, ending with a 2 or 3 m/m layer of compacted complex on top of the steel inserts. A quantity of teflon powder (approx. 10 cc) was then placed on top of the compacted powder and pressed at 28,000 pounds. The pressure being great enough, the teflon behaved essentially as a liquid and the complex was pressed into the slot under the hydrostatic pressure transmitted by the teflon. The resulting bars were dense and well shaped except at the teflon/complex interface which was concave, indicating that indeed a more uniform pressure distribution had been achieved than that found using a normal steel plunger. The uneven surface of the pressed bar was then ground flat. It is essential that the powder must be compacted sufficiently before introduction of the teflon powder to ensure that the teflon does not enter the bulk of the compact. Resistance measurements made with tungsten potential probes on all four sides of a pressed bar gave reproduceable and similar readings. This technique could well be used in the fields of metallurgy and semiconductor research to provide more uniformly pressed compacts, avoiding the density variations and anisotropy which so often occur. A previously pressed compact, possibly wrapped in this foil, immersed in teflon powder and then pressed at a high pressure would remove a great deal of these variations.

To establish if the acetonitrile is inert to the complex, conductivity

titration measurements were made. The stoichiometry of the I_2/Ph complex has been established by other workers³ as being 1.5 : 1. Thus, plotting the resistivity of acetonitrile containing one of the components (solution A) to which is added acetonitrile containing the second component (solution B) will provide a minimum resistivity when the solution contains $I_2: Ph$ in a 1.5 : 1 ratio. (This is assuming that the solvent is inert to the complex and that the initial conductivities of the two solutions are close enough to avoid dilution errors). The measurements made showed resistivity minimums occurring from 0.25 to 2 to 1 I_2/Ph ratios. Plotting the concentration of Ph/ml acetonitrile (solution A) vs. the resistivity minimum ratios established a definite relationship between these parameters showing that acetonitrile is not inert to the complex.

To assess the role of the various components of the cell, a split electrode assembly shown in Fig. was made. The outer split magnesium ring electrodes "A" and "C" have a free Mg area not in contact with the complex and the results indicate that it is this area which supports the majority of the current, the inner electrode "B" becoming almost completely passivated. The main point of this experiment was that it showed the C_2 to act merely as a contact to the complex which is, in fact, the cathode of a $Mg: Acetonitrile - I_2: Ph/I_2$ complete system. Table (a) and (b) give some results of these experiments.

Experiments are continuing to determine the cathode reaction and the role that acetonitrile plays.

REFERENCES

1. F. Gutman et al. J. Electrochemical Society, 114 323 (1967).
2. Y. Matsunaga, Helv. Phys. Acta 36 800 (1963).
3. F. Gutman and H. Keyzer, J. Chem. Phys. 46, 5, (1967).

TABLE (a)
CELL RESISTANCES (DRY)

$\begin{array}{c} C_2 \\ \diagdown \\ Mg \end{array}$	1	2	3
A	2900 Ω	2900 Ω	2900 Ω
B	2550 Ω	2550 Ω	2550 Ω
C	2700 Ω	2700 Ω	2700 Ω

ACETONITRILE ADDED

$\begin{array}{c} C_2 \\ \diagdown \\ Mg \end{array}$	1	2	3
A	52 Ω	68 Ω	50 Ω
B	290 Ω	215 Ω	285 Ω
C	75 Ω	84 Ω	89 Ω

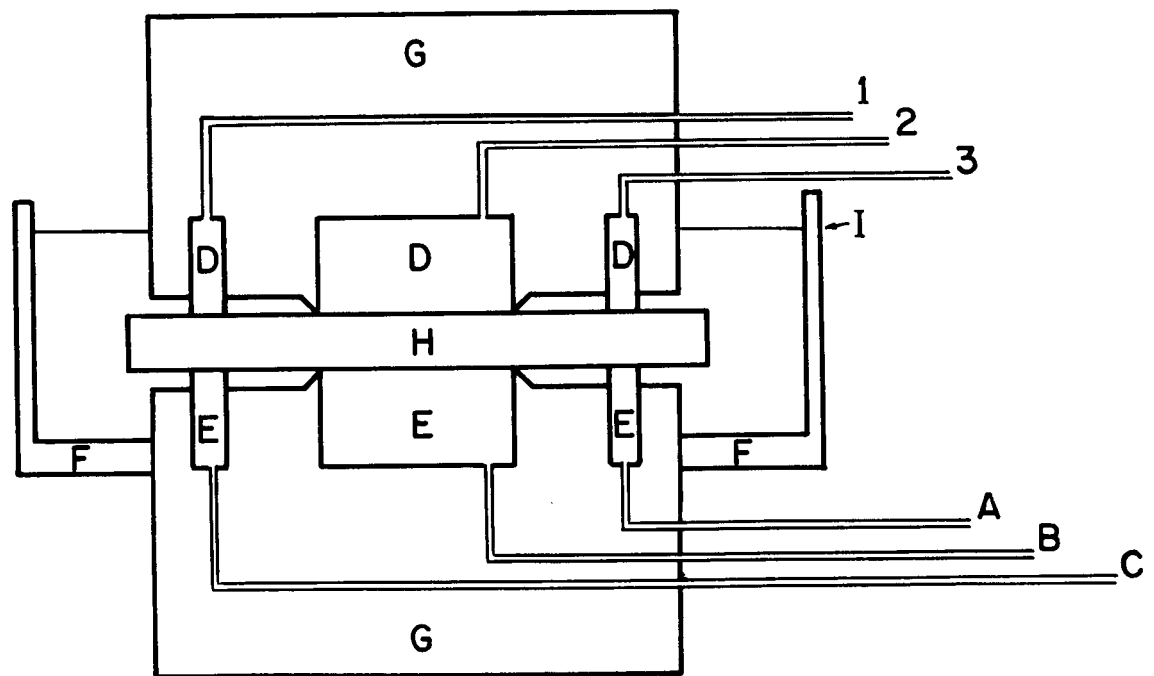
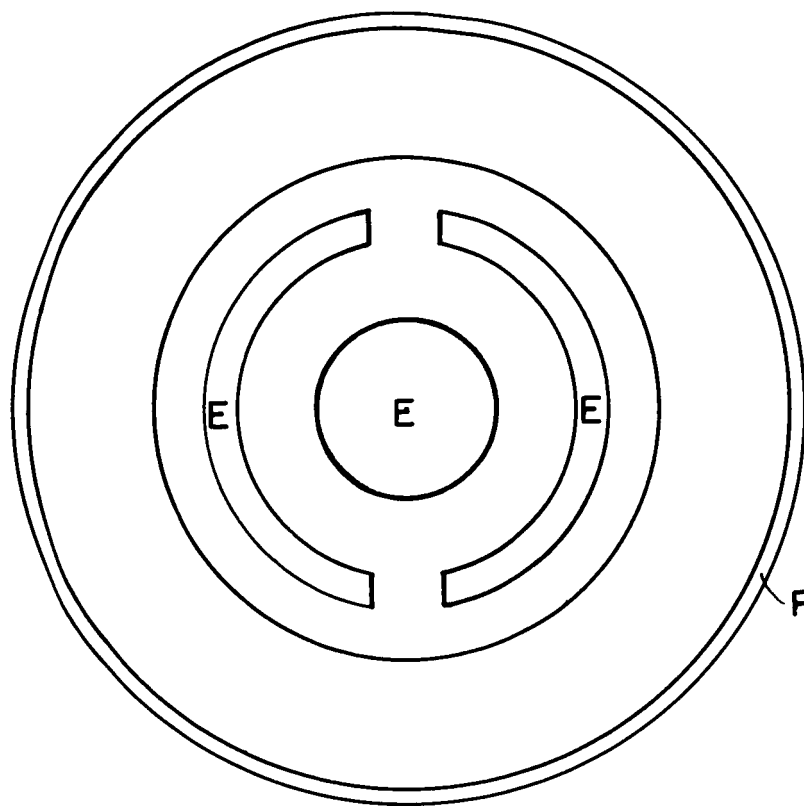
TABLE (b)

CURRENT DRAWN WITH 500Ω LOAD

Mg	vs. C_2	volts	I (ma)
A	1 + 2 + 3	1.3	3.9
B	1 + 2 + 3	0.55	2
C	1 + 2 + 3	0.92	3
A + B + C	1	1.32	4.5
A + B + C	2	1.3	4.5
A + B + C	3	1.3	4.5

CELL RESISTANCES AFTER DRAWING CURRENT
WITH 1000Ω LOAD FOR THREE HOURS

$\begin{matrix} C_2 \\ \diagdown \\ Mg \end{matrix}$	1 + 2 + 3	OCV
A	373Ω	1.0
B	860Ω	0.00
C	405Ω	1.54



Legend

A Lead to outer Mg electrode
 B Lead to central Mg electrode
 C Lead to outer Mg electrode
 D Carbon electrodes
 E Mg electrodes
 F Teflon cup

G Epoxy potting resin
 H Complex
 I Acetonitrile level
 1 = outer carbon electrode lead
 2 = inner carbon electrode lead
 3 = outer carbon electrode lead